

1 **Mouse Adaptation of Human Inflammatory Bowel Diseases Microbiota Enhances Colonization**
2 **Efficiency and Alters Microbiome Aggressiveness Depending on Recipient Colonic**
3 **Inflammatory Environment**

4 Simon M. Gray^{1,3}, Anh D. Moss^{1,5}, Jeremy W. Herzog³, Saori Kashiwagi^{3,6}, Bo Liu³, Jacqueline B.
5 Young⁵, Shan Sun⁵, Aadra Bhatt^{3,4}, Anthony A. Fodor^{2,5,*}, R. Balfour Sartor^{2,3,7,8,*}

6 ¹These authors contributed equally to this work.

7 ²These authors contributed equally to this work.

8 ³Center for Gastrointestinal Biology and Disease, Department of Medicine, Division of Gastroenterology
9 and Hepatology, University of North Carolina at Chapel Hill, Chapel Hill, NC, USA

10 ⁴Lineberger Comprehensive Cancer Center, University of North Carolina at Chapel Hill, Chapel Hill, NC,
11 USA

12 ⁵Department of Bioinformatics and Genomics, University of North Carolina at Charlotte, Charlotte, NC,
13 USA

14 ⁶Molecular Gastroenterology and Hepatology, Kyoto Prefectural University of Medicine, Kyoto, Japan

15 ⁷Department of Microbiology and Immunology, University of North Carolina at Chapel Hill, Chapel Hill,
16 NC, USA

17 ⁸National Gnotobiotic Rodent Resource Center, University of North Carolina at Chapel Hill, Chapel Hill,
18 NC, USA

19 *Correspondence: rbs@med.unc.edu. (R.B.S), afodor@uncc.edu (A.A.F)

20

21 **Abstract**

22 Understanding the cause vs consequence relationship of gut inflammation and microbial
23 dysbiosis in inflammatory bowel diseases (IBD) requires a reproducible mouse model of human-
24 microbiota-driven experimental colitis. Our study demonstrated that human fecal microbiota transplant
25 (FMT) transfer efficiency is an underappreciated source of experimental variability in human microbiota
26 associated (HMA) mice. Pooled human IBD patient fecal microbiota engrafted germ-free (GF) mice with
27 low amplicon sequence variant (ASV)-level transfer efficiency, resulting in high recipient-to-recipient
28 variation of microbiota composition and colitis severity in HMA *Il-10*^{-/-} mice. In contrast, mouse-to-
29 mouse transfer of mouse-adapted human IBD patient microbiota transferred with high efficiency and
30 low compositional variability resulting in highly consistent and reproducible colitis phenotypes in
31 recipient *Il-10*^{-/-} mice. Human-to-mouse FMT caused a population bottleneck with reassembly of
32 microbiota composition that was host inflammatory environment specific. Mouse-adaptation in the
33 inflamed *Il-10*^{-/-} host reassembled a more aggressive microbiota that induced more severe colitis in
34 serial transplant to *Il-10*^{-/-} mice than the distinct microbiota reassembled in non-inflamed WT hosts. Our
35 findings support a model of IBD pathogenesis in which host inflammation promotes aggressive resident
36 bacteria, which further drives a feed-forward process of dysbiosis exacerbated gut inflammation. This
37 model implies that effective management of IBD requires treating both the dysregulated host immune
38 response and aggressive inflammation-driven microbiota. We propose that our mouse-adapted human
39 microbiota model is an optimized, reproducible, and rigorous system to study human microbiome-driven
40 disease phenotypes, which may be generalized to mouse models of other human microbiota-modulated
41 diseases, including metabolic syndrome/obesity, diabetes, autoimmune diseases, and cancer.

42 **Keywords**

43 Inflammatory bowel diseases; experimental colitis; human microbiota associated mice; fecal microbiota
44 transplant; microbiota transfer efficiency; mouse-adapted; interleukin-10 deficient.

45

46 Main Body

47 Introduction

48 Human inflammatory bowel diseases (IBD) are heterogeneous chronic inflammatory conditions
49 driven by microbial activation of dysregulated intestinal immune responses in genetically susceptible
50 hosts¹. Host genetic susceptibility loci, such as polymorphisms in *Nod2*, *Il23r*, *Il-10r*, and *Il-10*, explain
51 <20% of IBD variance²⁻⁴ and disease incidence is rising globally⁵, suggesting that environmental factors
52 (diet, microbiome) are important drivers of IBD. IBD patients have altered intestinal microbiota
53 composition (dysbiosis), functionally characterized by reduced diversity, unstable community structure
54 over time and following perturbation, and expanded aggressive (*Gammaproteobacteria*,
55 *Enterococcaceae*, sulfur-reducing bacteria) but reduced beneficial (short-chain fatty acid [SCFA]-
56 producing *Clostridiales*, *Blautia*) resident bacteria⁶⁻¹⁰. Viable microbes are required to develop chronic
57 T-cell mediated intestinal inflammation in most experimental colitis models (i.e. *Il-10*^{-/-}, *Il2*^{-/-}, *Tcrab*^{-/-},
58 Naïve CD4⁺ T cell transfer to *Rag1/2*^{-/-}, *Tlr5*^{-/-}, *Tnf*^{ARE} mice) in which GF mice have no inflammation but
59 develop progressive intestinal inflammation after colonization with complex microbiota¹¹⁻¹⁶. Aggressive
60 resident bacteria (pathobionts) within the complex gut microbiota are the key drivers of intestinal
61 inflammation¹⁷⁻²²; however, whether dysbiotic expansion of pathobionts is a cause or consequence of
62 intestinal inflammation and how the host environment shapes microbial ecology in IBD remain poorly
63 understood.

64 Colonization of GF animals with defined human bacterial consortia or human fecal microbiota
65 transplant (FMT) are the gold-standard methods to demonstrate causality and investigate mechanisms
66 of human microbiome-driven disease phenotypes²³⁻²⁹. Defined consortia enable strict control of
67 microbiota composition, which facilitates mechanistic studies using genetically modified consortium
68 members but requires selection of bacterial strains by variable criteria^{28, 30-32}. Strain-level genetic and
69 functional variation are human disease-state specific, strongly impact host-microbe interaction, and
70 alter disease severity in experimental colitis models^{22, 33-38}. Because defined consortia may omit strain-
71 specific genetic and functional attributes responsible for human disease phenotypes, direct transplant

72 of human disease-associated feces to GF rodents is an appealing method to study human microbiome-
73 driven diseases.

74 Human IBD patient FMT to colitis-prone, GF mice (*Il-10*^{-/-} and *Rag1*^{-/-} T-cell transfer models)
75 transfers enhanced colitis severity compared to healthy patient FMT and induces a T_H17- and T_H2-
76 dominant immune phenotype that is characteristic of human IBD^{26, 39-42}. These fecal transplant studies
77 clearly transfer disease phenotype to susceptible mice by human IBD-associated microbes.
78 Importantly, human-to-mouse fecal transplant causes a microbial population bottleneck that engrafts a
79 compositionally distinct microbiome in recipient mice compared to human donor stool, likely due to low
80 human-to-mouse strain-level transfer efficiency (~40%) and host-specific microbe preferences⁴³⁻⁴⁶. We
81 took advantage of the microbiota reassembly associated with human-to-mouse FMT to ask if 1) the
82 host environment controls microbiota assembly and inflammatory potential, and 2) mouse-adaptation of
83 human fecal microbiota forms a microbial community that is stable in serial transplant to GF mice and
84 leads to more reproducible experimental phenotypes.

85 To evaluate the impact of the host inflammatory environment on gut microbiota assembly we
86 transferred pooled feces from human IBD patients with active disease to wild-type (WT) or *Il-10*^{-/-} mice.
87 Human microbiota-associated (HMA) *Il-10*^{-/-} mice had lower microbial alpha diversity, higher
88 compositional variability, and expansion of pathobionts compared to HMA WT mice, illustrating the
89 influence of an inflammatory colonic environment on dysbiosis. Serial transfer of non-inflamed (WT)
90 mouse-adapted human microbiota to GF *Il-10*^{-/-} mice induced less severe colitis than inflamed (*Il-10*^{-/-})
91 mouse-adapted human microbiota. Transplant of human fecal microbiota to GF mice resulted in low
92 human-to-mouse transfer efficiency at the strain level, while mouse-adapted human microbiota yielded
93 high strain level transfer efficiency. High microbiota compositional variability in HMA *Il-10*^{-/-} mice was
94 associated with variable colitis severity, but recipient mice colonized with mouse-adapted human
95 microbiota exhibited low compositional variability and more consistent colitis phenotypes. Our findings
96 suggest that the reproducibility and rigor of HMA animal studies are impacted by the variability of
97 human-to-mouse FMT; however, experimental design can be improved by first adapting the human

98 microbiota to the mouse host followed by transfer of mouse-adapted human microbiota for subsequent
99 highly reproducible mechanistic studies.

100 **Methods**

101 **Mouse Lines**

102 GF 129S6/SvEv background wildtype (WT) and *Il-10*-deficient (*Il-10*^{-/-}) mice¹³ were obtained from the
103 National Gnotobiotic Rodent Resource Center (NGRRC) at the University of North Carolina at Chapel
104 Hill. All animal experiments were conducted under approved Institutional Animal Care and Use
105 Committee protocols.

106 **Human fecal samples**

107 Human fecal samples from 5 adult patients with active Crohn's disease (CD) (4 donors) or ulcerative
108 colitis (UC) (1 donor) without prior intestinal surgery or antibiotic exposure within 3 months were
109 collected under an Institutional Review Board approved protocol (**Fig S1A**). De-identified stool samples
110 were aliquoted immediately after collection in an anaerobic chamber and stored without preservatives
111 at -80°C until use.

112 **Human fecal microbiota and mouse-adapted fecal microbiota colonization of GF mice**

113 Human fecal material from two sets of 3 human donors with active IBD (HM1: Donors 1, 2, 3; HM2:
114 Donors 3, 4, 5) was thawed and pooled in equal proportions by weight under anaerobic conditions
115 (N₂:H₂:CO₂ = 80:10:10), diluted with anaerobically reduced phosphate-buffered saline (PBS) to
116 generate a fecal slurry, and administered by 150µl oral gavage to recipient GF 129 WT or 129 *Il-10*^{-/-}
117 mice at 2mg pooled human donor stool per mouse. Mouse-adapted fecal pellets from HMA 129 WT or
118 129 *Il-10*^{-/-} mice were freshly collected and pooled daily between 14- and 21-days post-colonization and
119 frozen at -80°C without preservatives. To generate a standardized slurry of mouse-adapted microbiota,
120 mass collected fecal pellets from all mice in a group were pooled, homogenized, and diluted to
121 100mg/ml under anaerobic conditions in sterile anaerobically reduced lysogeny broth (LB) with 20%
122 glycerol. Solid particulate matter was pelleted by brief slow centrifugation and slurry supernatant was
123 aliquoted to cryovials for storage at -80°C. Slurry supernatant contains the same microbial community

124 composition as whole fecal material^{43, 47}. Mouse-adapted microbiota slurry generated as above from
125 fecal pellets of HMA 129 WT mice is called non-inflamed mouse adapted microbiota (NIMM), while
126 slurry generated from fecal pellets of HMA colitis-prone 129 *Il-10*^{-/-} mice is called inflamed mouse
127 adapted microbiota (IMM) (Fig 1A). To colonize GF mice with mouse-adapted microbiota, standardized
128 aliquots of 100mg/ml fecal slurry were thawed under anaerobic conditions, diluted with anaerobically
129 reduced PBS, and administered by oral gavage to recipient GF 129 WT or 129 *Il-10*^{-/-} mice at 2mg per
130 mouse in 150µl. Fecal pellets from IMM or NIMM associated 129 WT or 129 *Il-10*^{-/-} mice were collected
131 daily between 14- and 21-days post-colonization when the *Il-10*^{-/-} recipient microbiota has stabilized and
132 before cage effects are reported to develop^{48, 49}, processed and frozen in aliquots as above to generate
133 standardized slurries of serial passages (-g1, -g2, and -g3) of mouse-adapted microbiota (Fig 1A). All
134 experiments were performed using aliquots from a single production batch of mouse-adapted
135 microbiota. All mouse fecal transplant experiments were performed in BSL-2 isolation cubicles with
136 HEPA-filtered air on a 12-hour dark/light cycle with ad libitum access to autoclaved water and mouse
137 chow (Purina Advanced Protocol Select Rodent 50 IF/6F Auto Diet) using the sterile out-of-isolator
138 gnotobiotic cage technique (Complete cage GM500, Green Line, Tecniplast)⁵⁰. Cage changes and all
139 animal handling were performed in a laminar flow biosafety cabinet under sterile technique following
140 ultraviolet light treatment and 10-minute Peroxigard sterilization of all equipment and surfaces. We
141 maintained strict GF conditions with the out-of-isolator gnotobiotic technique for at least 2 weeks. We
142 consider the complex microbiota fecal transplant experiments reported here to be 'near-gnotobiotic'
143 with low risk of environmental contamination, but not strictly gnotobiotic since they are performed with
144 out-of-isolator gnotobiotic cage technique for durations >2 weeks and sterility could not be monitored
145 due to complex microbiota transplants.

146 **Gene expression by qRT-PCR, Intestine histopathology score, and Fecal lipocalin-2**
147 **quantification**

148 Standard molecular assays and histopathology scoring were performed as previously described⁵¹⁻⁵³.
149 Details of these procedures and a list of qPCR primers are found in the Supplemental Experimental
150 Procedures.

151 **Statistical Analyses**

152 Non-sequencing based statistical analyses were performed with Prism 10 (GraphPad) with statistical
153 tests and significance thresholds indicated in figure legends.

154 **16S rRNA Amplicon Metagenomic Sequencing and Analysis**

155 16S rRNA amplicon (variable regions 3-4) sequencing was performed on the Illumina NextSeq 2000
156 platform, processed, and taxonomically classified through QIIME2 by the UNC Microbiome Core⁵⁴.
157 Additional details of these procedures are found in the Supplemental Experimental Procedures.
158 Sequence counts data at both the genus and phylum level were extracted from the respective QIIME2
159 artifact files. The amplicon sequence variant (ASV)-level counts table was generated with forward reads
160 using the following parameters with single-end DADA2 on the QIIME2 (version 2021.2) platform: the
161 first 10 base pairs of each sequence were trimmed, and the sequences were truncated to 180 base
162 pairs as determined by sequence quality using FastQC (version 0.11.9)^{54, 55}. Statistical analysis was
163 conducted with the *vegan* package (ver.2.6-2) in R (ver. 4.2.2) and visualized with the Shiny application
164 *Plotmicrobiome* and custom R code (Sun et al. GitHub <https://github.com/ssun6/plotmicrobiome>,
165 **Supplemental File 1**). To ensure reproducibility and rigor, the results of our analyses were
166 independently reproduced with custom Python code by a second bioinformatician (JBY) with replicated
167 key figures and reproducible tested code available in a Jupyter Notebook file (**Supplemental File 1**). R
168 and Python code used in our analyses are available at [https://github.com/anhmoss/Mouse-Adaptation-
169 of-Human-Inflammatory-Bowel-Disease-Microbiota-Enhances-Colonization-Efficiency](https://github.com/anhmoss/Mouse-Adaptation-of-Human-Inflammatory-Bowel-Disease-Microbiota-Enhances-Colonization-Efficiency) and in
170 **Supplemental File 1**. 16S rRNA amplicon sequencing data are available at
171 [https://github.com/anhmoss/Mouse-Adaptation-of-Human-Inflammatory-Bowel-Disease-Microbiota-
172 Enhances-Colonization-Efficiency](https://github.com/anhmoss/Mouse-Adaptation-of-Human-Inflammatory-Bowel-Disease-Microbiota-Enhances-Colonization-Efficiency).

173 To account for varying sequencing depth, all counts data were normalized according to the
174 following formula prior to downstream statistical analyses:

$$175 \log_{10} \left(\frac{\text{raw OTU count for sample}_i}{\text{total sequences for sample}_i} \times \text{average sequence depth} + 1 \right)$$

176 This formula adjusts the pseudo-count to have a similar effect across samples by scaling all
177 samples to the average sequencing depth. ASV transfer efficiency was measured as Pearson
178 correlation coefficient (r) for pairs of samples within a given group or between two groups.

179 Results

180 **Mouse-adapted human microbiota induces more consistent and reproducible colitis than** 181 **directly transplanted human microbiota.**

182 Human fecal microbiota transplantation into GF mice can transfer microbe-dependent
183 pathological phenotypes to recipient animals, allowing investigation of microbial mechanisms of human
184 diseases such as IBD^{23, 26, 56}. The large interpersonal variation of human gut microbiota, host-specificity
185 of gut microbial ecology, and variable engraftment of human gut microbes into GF mice pose
186 challenges to transplanted phenotype reproducibility and interpretation^{43, 45, 46, 57}. To understand the
187 impact of recipient host environment on human fecal microbiota engraftment and phenotype transfer in
188 a mouse model of experimental colitis, we transplanted pooled feces from 3 humans with active IBD (2
189 CD, 1UC) to non-inflamed WT or colitis-susceptible *Il-10*^{-/-} GF mice (Fig 1A, S1A). We then
190 transplanted these mouse-adapted microbiota to sequential cohorts of non-inflamed WT or colitis-
191 susceptible *Il-10*^{-/-} GF recipient mice, generating serial transfers of mouse-adapted human microbiota
192 identified as -g1, -g2, and -g3 (Fig 1A). In our nomenclature, different human IBD patient fecal pools are
193 called Human Microbiota (HM1 or HM2) (shown in S1A), feces from HMA WT mice are called Non-
194 Inflamed Mouse-adapted Microbiota (NIMM), and feces from HMA *Il-10*^{-/-} mice are called Inflamed
195 Mouse-adapted Microbiota (IMM) (Fig 1A). Serial mouse-adapted fecal transplant experiments were
196 only conducted with HM1-derived HMA mouse stool due to resource constraints; HM1 was selected
197 because the cohort contained both UC and CD donors (Fig 1A; S1A). Because colonic immune

198 stimulation of GF mice is equivalent following transplant of human or mouse microbiota, HMA mice are
199 a clinically relevant model of experimental colitis^{44, 45}.

200 GF 129 WT mice receiving HM1, NIMM-g1, or NIMM-g2 fecal transplant did not develop colitis
201 as assessed by colon histology, non-invasive fecal lipocalin-2 (f-LCN2), and tissue inflammatory
202 cytokine levels (Fig 1B-D; S1B-C). Transplantation of both human microbiota HM1 and mouse-adapted
203 microbiota IMM-g1 or IMM-g2 to GF 129 *Il-10*^{-/-} mice induced severe colitis as assessed by colon
204 histology, non-invasive f-LCN2, and inflammatory cytokine levels (Fig 1C-F; S1B,D). IMM-g1 and IMM-
205 g2 induced cecal predominant colitis that was equivalent in severity and kinetics to colitis induced by
206 HM1 (Fig 1E; S1B,D). However, HM1 induced colitis was more variable than IMM-g1 or IMM-g2
207 induced colitis as quantified by segment and total histology score variance and interquartile range (Fig
208 1E; Fig S1G). The high phenotypic variance of human microbiome-induced colitis was replicated by a
209 separate cohort (HM2) of pooled feces from 3 humans with active CD transplanted to *Il-10*^{-/-} GF mice
210 (Fig S1E,F). In contrast to the highly variable phenotype of human microbiome-induced colitis, mouse-
211 adapted microbiome IMM-g1 induced colitis had little variation in severity or distribution within or across
212 independent experiments (Fig 1E,F; S1G,H). To evaluate whether variability in colitis phenotype was
213 related to microbiome composition, we performed 16S amplicon sequencing of input donor microbiota
214 and fecal samples collected from ex-GF 129 WT and 129 *Il-10*^{-/-} mice colonized for 28 days with human
215 microbiota or mouse-adapted microbiotas (Fig 1A). As we show later in the results (Fig 3), human
216 microbiota transplant to GF mice was associated with significantly lower microbiota engraftment
217 consistency than mouse-adapted microbiota transplant, suggesting that variability in engrafted human
218 microbiota composition may cause variability in colitis phenotypes.

219 **Human microbiome restructures with transplant to GF mice.**

220 To investigate how the recipient host intestinal environment shapes human microbiota
221 engraftment in GF mice, we assessed microbiome compositional variation by calculating the average
222 relative abundance of genera across all samples for each fecal transplant condition. Fig 2 shows
223 taxonomic barplots of the 8 most abundant genera across groups with the remaining lower abundance

224 taxa grouped as “Other” (Fig 2, S2A). The 30 most abundant genera across groups and the relative
225 abundance of genera for individual mice are visualized in barplots in Fig S2. We performed pairwise t-
226 tests to assess differential abundance between groups, excluding genera present in less than 10% of
227 the samples (Table S1).

228 Pooled human microbiome composition (HM1 input and HM2 input) was compositionally distinct
229 from all colonized mouse groups as visualized by taxonomic barplots and principal coordinates analysis
230 (PCoA) clustering (aka multidimensional scaling), with the strongest separation existing between
231 human and mouse-adapted microbiotas along the first MDS axis (Fig 2, 3A). Compared to human
232 microbiomes, HMA mouse and MA-FMT mouse microbiomes had increased relative abundance of
233 *Akkermansia*, *Lachnoclostridium*, *Ruminococcus gnavus* group, and *Hungatella*, a low-abundance
234 member of the human gut that was not detectable by 16S in HM1 or HM2 inputs (Fig 2). *Bacteroides*, a
235 major constituent of the human gut microbiome, was present in HM1 input and HM2 input, and
236 expanded in HM2-associated *Il-10*^{-/-} mice but reduced in HM1-associated WT and *Il-10*^{-/-} mice (Fig 2,
237 Table S1). The expansion of *Bacteroides* in HM2- but reduction in HM1-associated *Il-10*^{-/-} mice was
238 surprising because *Bacteroides* was more abundant in HM1 input compared to HM2 input, suggesting
239 stochastic factors influence engraftment of human microbiota in GF mice (Fig 2). These data
240 demonstrate that human microbiota association of GF mice results in major compositional restructuring
241 of the engrafted microbiome that may be partially stochastic.

242 **Recipient host environment influences engraftment composition of human-microbiota** 243 **associated mice.**

244 The recipient host environment shapes the engrafted microbiome composition of HMA mice (Fig
245 2, S2, 3A, B). After removing HM1 and HM2 inputs, PCoA showed separation of inflamed mouse-
246 adapted microbiota (IMM) and non-inflamed mouse-adapted microbiota (NIMM) along the first MDS
247 axis (Fig 3B). PERMANOVA test with all mouse recipient groups as the model term demonstrated that
248 approximately 43% of the variation in the data is explained by the recipient host environment
249 (coefficient of determination, $R^2 = 0.43$, $p=0.001$). Mouse adaptation in the inflamed *Il-10*^{-/-} host (IMM)

250 enriched for significantly higher relative abundance of *Escherichia-Shigella*, *Parasutterella*,
251 *Enterococcus*, *Clostridium_sensu_stricto_1*, *Ruminococcus gnavus* group, and *Bifidobacterium* but
252 significantly lower relative abundance of *Clostridium innocuum*, *Blautia*, *Lachnoclostridium*, and multiple
253 other genera within *Lachnospiraceae* and *Ruminococaceae* when compared to mouse adaptation in the
254 non-inflamed WT host (NIMM) (Fig 2, S2, Table S1). PCoA of serial microbiota passage within the non-
255 inflamed WT host environment (NIMM-g1, -g2) showed that the global microbiome structure remained
256 stable with no distinct clustering of groups (Fig 3D) and only 7 operational taxonomic units (OTUs)
257 demonstrated significantly differential abundance between NIMM-g1 and -g2 using a cutoff of FDR<0.1
258 (Fig 2, S2, Table S1). PCoA of serial microbiota passage within the inflamed *Il-10^{-/-}* host environment
259 (IMM-g1, -g2) similarly showed globally stable microbiome structure with no distinct clustering of groups
260 (Fig 3C, S3A), while no OTUs were differentially abundant between IMM-g1 and -g2 (Fig 2, S2, Table
261 S1). Mouse adaptation in the inflamed *Il-10^{-/-}* host (IMM) was associated with significantly lower alpha
262 diversity at the amplicon sequence variant (ASV) level compared to the non-inflamed WT host (NIMM),
263 consistent with observations that human IBD patients have lower alpha diversity than healthy humans
264 (Fig 3E, S3B,C)⁸. Together, these data demonstrate that the composition of the human microbiome is
265 fundamentally restructured with transplant to GF mice and that the recipient host environment strongly
266 shapes the relative abundance of engrafted strains with the inflamed *Il-10^{-/-}* host (IMM) driving a
267 dysbiotic microbiome defined by lower alpha-diversity, enrichment of pathobionts, and reduction of
268 protective SCFA-producing bacteria relative to the non-inflamed WT host (NIMM).

269 **Human microbiota engrafts with variable composition compared to more consistent**
270 **engraftment by mouse-adapted microbiota.**

271 Since the human microbiome restructures with transplant to GF mice, we speculated that
272 variability in engrafted microbiota composition may explain the colitis phenotype variability of HMA *Il-10^{-/-}*
273 mice (Fig 1E, S1E-F). Variability of microbiota composition was quantified by pairwise calculation of
274 Pearson correlation coefficient for all samples within the same group (i.e., all mice within HM1->KO). A
275 high Pearson correlation coefficient indicates compositional similarity between samples in a group,

276 while a low coefficient indicates compositional variability between samples in a group. Human
277 microbiota transplant to 129 *Il-10^{-/-}* mice (HM1->KO) was associated with significantly lower Pearson
278 correlation coefficients than mouse-adapted microbiota transplants to 129 *Il-10^{-/-}* mice (IMM-g1->KO,
279 IMM-g2->KO) (Fig 3F, S3D). A similar trend was seen with human microbiota or mouse-adapted
280 microbiota transplant to 129 WT mice (Fig 3F). Pearson correlation coefficients for 129 *Il-10^{-/-}* recipient
281 mice were consistently lower than 129 WT recipients at each stage of serial passage (i.e., HM1->WT vs
282 HM1->KO or NIMM-g1->WT vs IMM-g1->KO), demonstrating that inflammation promotes variability of
283 microbiome composition while health is associated with microbiome stability (Fig 3F). These results are
284 consistent with observations in humans that the composition of IBD patient microbiomes fluctuate more
285 than healthy controls over time^{28, 58}. Together, these data suggest that 1) inflammation promotes
286 microbiome variability and 2) variability in colitis phenotype with human microbiota transplant may be
287 due to variability in engrafted human microbiota composition, while the more consistent colitis induced
288 by mouse-adapted microbiota may be due to homogeneity of engraftment of mouse-adapted
289 microbiota.

290 **Mouse-adapted human IBD microbiota transfers with higher efficiency than human fecal**
291 **transplant.**

292 Since HMA mice had significantly different microbiome composition than human donor stool but
293 mouse-adapted FMT mice had highly consistent microbiomes between serial transfer, we evaluated
294 whether mouse-adapted microbiota transfers to GF mice more efficiently than human fecal transplant
295 (Fig 4A-D). To quantify transfer efficiency, we detected all ASVs across all samples and compared ASV
296 abundance between human stool, HMA mice, and mouse-adapted FMT mice across serial transfers
297 (Fig 4A-D). We visualized these data using scatter plots where each dot represents a unique ASV
298 plotted by log₁₀ relative abundance in the input microbiome (x-axis) vs recipient mouse microbiome (y-
299 axis). We quantified transfer efficiency using Pearson correlation coefficient (r), where high Pearson r
300 indicates consistent ASV abundances between samples and high transfer efficiency. We used deep
301 16S amplicon sequencing rather than whole genomic shot gun sequencing (WGS) because repeat

302 sequencing of the same region allows for exact identification of ASVs in a database-independent
303 manner without reliance on classification algorithms.

304 Human fecal transplant to WT or *Il-10^{-/-}* mice was associated with low transfer efficiency and
305 poor transfer of relative composition to recipient mice (Fig 4A-D, S5D-E). Very similar results were seen
306 in WT and *Il-10^{-/-}* mice. A large proportion of ASVs present in human stool did not transfer to recipient
307 mice, which is illustrated by ASVs falling on the x-axis (Fig 4A,C). The relative abundance (\log_{10}
308 normalized) of non-transferring ASVs demonstrated that even moderately to highly abundant ASVs in
309 human stool did not transfer efficiently to GF mice (Fig 4E,H). ASV relative abundance in human stool
310 had little correlation with relative abundance in recipient mice (Fig 4A,C), leading to a very low ASV
311 level transfer efficiency for human fecal transplant to WT ($r=0.34\pm 0.03$) or *Il-10^{-/-}* ($r=0.33\pm 0.03$) mice
312 (Fig 4B,D). For mouse-adapted FMT, however, ASV relative abundance in MA-FMT input (IMM or
313 NIMM) was highly correlated with relative abundance in recipient mice (Fig 4A,C). Only a small
314 proportion of ASVs present in mouse-adapted microbiota did not transfer to recipient mice, and those
315 non-transferring ASVs were primarily low-abundance strains (Fig 4A,C,F-G,I-J). Serial transfer of
316 mouse-adapted microbiota further improved the correlation between input and recipient microbiomes
317 and reduced non-transferring ASV numbers, leading to very high ASV level transfer efficiency for
318 mouse-adapted FMT to WT ($r=0.84\pm 0.02$) or *Il-10^{-/-}* mice ($r=0.85\pm 0.05$) (Fig 4 A-D). Similar results were
319 found when comparing human microbiome input to mouse-adapted microbiome inputs (Fig S4A-F).
320 Analysis of transfer efficiency at the genus level also demonstrated low transfer efficiency for human
321 fecal transplant but high transfer efficiency for mouse-adapted FMT; however, phylum level analysis
322 showed high transfer efficiency for all conditions, giving a misleading perception of transfer efficiency
323 (Fig 5A-H, S5F).

324 Some ASVs (falling on the y-axis) in HMA mice were not detected in human stool, representing
325 either mutation of the V3-V4 sequence, *in vivo* expansion of very low abundance strains undetected at
326 the depth of 16S sequencing utilized, or environmental contamination (Fig 4A,C). To rule out

327 environmental contamination, we performed human FMT to GF mice in strictly gnotobiotic isolators and
328 still detected many ASVs in HMA mice that were not detected in human input stool by 16S Seq (Fig
329 S5D-E). We analyzed an independently published 16S Seq dataset of HMA WT mice colonized and
330 then bred in a gnotobiotic isolator and found similar results of low human-to-mouse but high mouse-
331 adapted-to-offspring mouse transfer efficiency at the ASV level (Fig S5A-C)⁴⁴. These data demonstrate
332 that a large fraction of the human microbiome does not efficiently engraft GF mice; however, once
333 engrafting strains adapt to the mouse gut they transfer with very high efficiency in serial fecal
334 transplant.

335 **Transfer efficiency varies between taxa.**

336 To assess the transfer efficiency of different taxa from transplant of human microbiota or
337 mouse-adapted microbiota to GF mice, we compared Pearson correlation coefficients (r) between phyla
338 (Fig 5I-N). Unclassified bacteria had the lowest transfer efficiency in all groups, consistent with prior
339 reports (Fig 5I-N)⁴³. *Verrucomicrobiota* and *Fusobacteriota* consistently had very high transfer
340 efficiency, which likely reflected that a single species from each phylum was present in donor stool (Fig
341 5I-N). *Akkermansia muciniphila*, a known keystone species, is the only human gut member of
342 *Verrucomicrobiota* and transferred highly efficiently across all transplant conditions and recipients.
343 Transfer efficiencies trended lower for *Firmicutes*, *Bacteroidota*, and *Actinobacteriota* and trended
344 somewhat lower in *Proteobacteria* in all *Il-10*^{-/-} mice compared to WT mice (Fig 5I-N).

345 **Inflamed mouse-adapted microbiome induces faster onset colitis than non-inflamed mouse** 346 **adapted microbiome.**

347 Since mouse-adaptation of human microbiota in the non-inflamed (WT) host reduced the
348 frequency of pathobionts while expanding putatively protective bacteria, we investigated whether
349 NIMM-g1 induces less severe colitis than IMM-g1 when transplanted to *Il-10*^{-/-} GF mice (Fig 6A). At 14
350 days post-colonization, NIMM-g1 colonized *Il-10*^{-/-} mice had significantly lower f-LCN2 levels, cecum-
351 and total colon histologic inflammation than IMM-g1 colonized *Il-10*^{-/-} mice (Fig 6B, S6A-B). At 28 days
352 post-colonization, NIMM-g1 colonized *Il-10*^{-/-} mice continued to have significantly reduced cecal

353 inflammation scores and trend toward lower cecal inflammatory cytokine levels but had developed
354 increased rectal inflammation compared to IMM-g1 colonized *Il-10^{-/-}* mice (Fig 6C). NIMM-g1 colonized
355 *Il-10^{-/-}* mice had significantly lower maximum segment inflammation on a per-mouse basis compared to
356 IMM-g1 colonized *Il-10^{-/-}* mice (Fig 6C). However, the increase in rectal inflammation resulted in a non-
357 significant trend toward lower f-LCN2 levels and no difference in total colon histology scores between
358 NIMM-g1 and IMM-g1 colonized *Il-10^{-/-}* mice at 28 days post-colonization (Fig 6C; S6C). PCoA
359 demonstrated that the microbiome of NIMM-g1 colonized *Il-10^{-/-}* mice (NIMM-g1->KO) clustered with
360 WT HMA and MA-FMT mice, rather than *Il-10^{-/-}* HMA or MA-FMT mice (Fig 6E). Alpha diversity of
361 NIMM-g1 colonized *Il-10^{-/-}* mice was equal to NIMM-g1 colonized WT mice and non-significantly higher
362 than IMM-g1 colonized *Il-10^{-/-}* mice (Fig 6G). These data suggest that major changes in community
363 restructuring occur during initial adaptation of human microbiota to the non-inflamed mouse host, but
364 that once a stable mouse-adapted community forms it transfers with stable global structure in serial
365 transplant to subsequently inflamed GF host mice. Although PCoA demonstrated that global
366 microbiome structure of NIMM was stable between the inflamed and non-inflamed environments,
367 taxonomic bar plots and differential abundance analysis demonstrate that several taxa undergo
368 changes in frequency (Fig 6F; S6D; Table S1). Putatively protective *Blautia* and *Lachnospiraceae*
369 *NK4A136* group were significantly reduced while the pathobiont containing genera *Ruminococcus*
370 *gnavus* group and *Hungatella* were significantly expanded in *Il-10^{-/-}* compared to WT mice colonized
371 with NIMM-g1, suggesting that these genera may be particularly responsive to the inflammatory
372 environment – consistent with observations in human IBD microbiome profiling studies (Fig 6F, S6E-
373 H)^{7, 9, 59, 60}. Together, these data demonstrate that human microbiome adaptation is dependent on the
374 host environment, but once a stable mouse-adapted microbiome has been established it remains
375 remarkably stable in composition despite an altered host environment.

376

377 Discussion

378 The role of gut microbiota dysbiosis as cause or consequence of intestinal inflammation is an
379 area of active investigation and debate with clinical importance for the management of IBD¹. Transplant
380 of human disease-associated feces to GF rodents is an approach that captures strain-specific
381 functional and genetic variation responsible for human-microbiome driven disease phenotypes without
382 biased selection of defined input strains. Although widely accepted, this approach is complicated by
383 phenotypic and experimental variability of unclear etiology. Our study identified that FMT transfer
384 efficiency is an underappreciated source of experimental variability. Using high depth, low-error rate
385 Illumina 16S amplicon sequencing (16S Seq), we showed that pooled human IBD patient fecal
386 microbiota engrafts GF mice with low ASV-level transfer efficiency, resulting in high recipient-to-
387 recipient variation of microbiota composition and colitis severity in HMA *Il-10*^{-/-} mice. Human-to-mouse
388 FMT caused a population bottleneck with reassembly of microbiota composition that was host
389 inflammatory environment specific. In the inflamed environment of HMA *Il-10*^{-/-} mice, the microbiota
390 reassembled with lower microbial alpha diversity, higher recipient-to-recipient microbiota compositional
391 variability, and expansion of pathobionts compared to the distinct microbiota reassembled in the non-
392 inflamed environment of HMA WT mice. Following the initial human-to-mouse population bottleneck
393 and microbiota reassembly, the mouse-adapted human IBD patient microbiota transferred with high
394 efficiency and low compositional variability to GF recipients, which correlated with highly consistent and
395 reproducible colitis phenotypes in *Il-10*^{-/-} recipient mice. The mouse-adapted microbiota composition
396 was remarkably stable in serial transplant to both inflamed and non-inflamed host environments. We
397 replicated the key finding of low human-to-mouse but high mouse-adapted-to-mouse transfer efficiency
398 at the ASV level by analysis of an independently published 16S Seq dataset of HMA WT mice bred in a
399 gnotobiotic isolator⁴⁴. Microbiota adaptation in the inflamed environment assembled a more aggressive
400 microbiota than adaptation in the non-inflamed environment, demonstrating that the genetically
401 determined host inflammatory environment shapes dysbiosis that subsequently drives more severe
402 inflammation. Our data demonstrate that host gut inflammation is both a cause and consequence of
403 microbial dysbiosis.

404 Our data support recent criticism that stochastic ecological processes and donor heterogeneity
405 influence phenotypes in HMA murine models⁶¹. We found that OTU based metrics, especially at higher
406 taxonomic levels, over-estimated transfer efficiency compared to ASV analysis^{23, 44, 61}. The low transfer
407 efficiency and population bottleneck of human-to-mouse FMT led to high variability in engrafted
408 microbiota composition between individual recipients of the same human input stool, which correlated
409 with significant variability in colitis severity in recipient *Il-10^{-/-}* mice. We speculate that stochastic
410 differences in engraftment were accentuated by the bottleneck of human-to-mouse FMT and drove
411 phenotypic variability⁶¹. Large interindividual variability of human donor microbiota likely exacerbates
412 this phenomenon in HMA murine studies^{8, 57, 61}. We used pooled human IBD donor stool to mitigate the
413 impact of individual human donor microbiota heterogeneity and replicated our results with 2 pooled
414 human donor pools. Our pooling approach is suitable for experimental designs that require a
415 representative human disease associated microbiome to interrogate mechanistic questions (i.e., the
416 impact of diet or host genetic background) or test therapeutics (i.e., live biotherapeutics or novel
417 biologics); however, studies evaluating microbiome-driven phenotype transfer require an appropriately
418 powered number of individual human donors to establish causality and avoid bias from pseudo-
419 replication⁶¹. In our study, both pooled human fecal cohorts HM1 and HM2 contained *Bacteroides*
420 genus at high abundance. However, following human-to-mouse transplant, *Bacteroides* abundance
421 dramatically decreased in HM1 recipients but expanded in HM2 recipients. Although our study was not
422 powered to distinguish whether this divergent engraftment arose from microbial ecology of the donor
423 microbiota or stochastic processes, our data suggest that low human-to-mouse transfer efficiency in the
424 setting of donor heterogeneity and stochastic ecological processes is an underappreciated source of
425 variability in HMA animal models. In contrast, transplant of mouse-adapted human microbiota yielded
426 highly reproducible and consistent microbiota composition and colitis phenotypes – an improved model
427 for studying human microbiota driven diseases.

428 Our data demonstrated that mouse-adaptation of human fecal microbiota was shaped by the
429 host inflammatory environment to form stable microbial communities that reproducibly engrafted GF

430 mice with high efficiency to drive distinct colitis phenotypes. Mouse-adaptation in the inflamed
431 genetically susceptible host assembled an aggressive microbiota with low alpha-diversity and high
432 pathobiont abundance (*Enterobacteriaceae*, *R. gnavus*) that drove more severe colitis in serial
433 transplant to *Il-10*^{-/-} mice than microbiota adapted in the non-inflamed host. Gut inflammation induces
434 host-derived metabolites, such as nitrate, lactate, and ethanolamine, that enhance fitness, abundance,
435 and virulence of aggressive *E. coli* and promote ectopic gut colonization of inflammation-associated
436 *Veillonella* species⁶²⁻⁶⁶. Adherent and invasive *E. coli* and other inflammation-associated aggressive
437 resident bacteria drive intestinal inflammation in murine colitis models^{1, 18, 19, 21}. Together with the
438 literature, our data support a model of IBD pathogenesis in which host inflammation in genetically
439 susceptible hosts promotes the expansion, fitness, and virulence of aggressive resident bacteria, which
440 further drive a feed-forward process of dysbiosis exacerbated gut inflammation. This model implies that
441 effective management of IBD requires treating both the dysregulated host immune response and
442 aggressive inflammation-associated microbiota.

443 Our study benefitted from several strengths including an experimental design that incorporated
444 multiple serial FMT, high recipient mouse numbers, and application of high-depth low error rate
445 sequencing for accurate ASV tracking; however, there were some limitations. First, most experiments
446 were conducted in out-of-isolator gnotobiotic cages, where contamination risk is extremely low but
447 could not be monitored due to the complex FMT inputs. To address this, we replicated key experiments
448 in strict gnotobiotic isolators, confirming our findings of low human-to-mouse ASV-level transfer
449 efficiency and the emergence of ASVs in HMA mice not detected in human input stool. Second, we did
450 not analyze WGS data to compare transfer efficiency of microbial functions vs taxonomic composition.
451 We used 16S Seq rather than WGS because repeat sequencing of the same region allows for exact
452 identification of ASVs in a database-independent manner without reliance on classification algorithms.
453 Future WGS studies are needed to evaluate the impact of taxonomic transfer efficiency on transfer of
454 microbial functions. Third, we did not evaluate the impact of mouse diet on the initial human-to-mouse
455 engraftment bottleneck – an important topic for follow up studies.

456 Our mouse-adapted human microbiota model is an optimized, reproducible, and rigorous
457 system to study human microbiome-driven disease phenotypes. Multiple approaches (human
458 microbiome profiling, defined consortia animal studies, HMA animal models) can investigate causality
459 and identify mechanisms of microbiota-driven diseases^{1, 29, 67}. Mono-association and defined
460 consortium studies are reductionist approaches where a single variable (i.e., single-gene mutations)
461 can interrogate bacterial mechanisms^{1, 29}. Representative synthetic microbiota, such as hCOM2,
462 PedsCom, and SIHUMI, provide a more ecologically complex system with known input strain identity
463 and the ability to easily track relative abundance by simplified metagenomic sequencing approaches^{28,}
464 ^{31, 32, 67, 68}. However, even large complex defined consortia do not capture the understudied strain level
465 variation that exists in heterogeneous human resident microbiota and contributes to important
466 differences in strain dependent microbiota aggressiveness^{22, 36, 37, 66}. The high transfer efficiency of
467 mouse-adapted human microbiota transplant to GF mice improves phenotype consistency, experiment
468 reproducibility and rigor of mouse models of human microbiota-driven disease. Homogenous
469 repositories of mouse-adapted human microbiota provide an identical microbial starting point for every
470 experiment that can be replicated over time and between institutions/collaborators without transfer of
471 human host genetic material present in human feces to collaborators^{69, 70}. Because of high transfer
472 efficiency and reproducible engraftment, mouse-adapted human microbiota repositories can be
473 expanded *in vivo* when stocks run low, mitigating limitations of finite human fecal samples. While this
474 study focused on colitis, our mouse-adapted human microbiota approach is a framework that may be
475 generalized to mouse FMT models of other human microbiota-modulated diseases, such as metabolic
476 syndrome/obesity, diabetes, autoimmune diseases, and cancer.

477

478 **Acknowledgements**

479 We thank the members of the Sartor and Fodor laboratories for helpful comments, suggestions, and
480 support. This study was supported in part by NIH/NIDDK T32DK007737 (SMG), P01DK094779 (RBS),
481 P40OD010995 (RBS), CGIBD P30DK034987 (RBS), Crohn's & Colitis Foundation Gnotobiotic Facility

482 (RBS), UNC Physician Scientist Training Program Fellowship Award (SMG), Crohn's & Colitis
483 Foundation Career Development Award (SK). We thank the staff and manager, Josh Frost, of the
484 National Gnotobiotic Rodent Resource Center for gnotobiotic husbandry and mice. The UNC
485 Microbiome Core is funded in part by the UNC Nutrition Obesity Research Center (NORC P30
486 DK056350).

487 **Competing Interests**

488 None relevant to this study. RBS receives grant support from Gusto Global LLC, Biomica, and
489 ImmunityX, and serves on the Scientific Advisory Board of Biomica.

490 **Data Availability Statement**

491 The datasets, R code, and Python code are publicly available at [https://github.com/anhmoss/Mouse-](https://github.com/anhmoss/Mouse-Adaptation-of-Human-Inflammatory-Bowel-Disease-Microbiota-Enhances-Colonization-Efficiency)
492 [Adaptation-of-Human-Inflammatory-Bowel-Disease-Microbiota-Enhances-Colonization-Efficiency](https://github.com/anhmoss/Mouse-Adaptation-of-Human-Inflammatory-Bowel-Disease-Microbiota-Enhances-Colonization-Efficiency) and
493 from the corresponding authors upon reasonable request.

494

495 **References**

- 496 1. Sartor RB, Wu GD. Roles for Intestinal Bacteria, Viruses, and Fungi in Pathogenesis of
497 Inflammatory Bowel Diseases and Therapeutic Approaches. *Gastroenterology*. 2017;152(2):327-39.e4.
- 498 2. Jostins L, Ripke S, Weersma RK, Duerr RH, McGovern DP, Hui KY, et al. Host-microbe
499 interactions have shaped the genetic architecture of inflammatory bowel disease. *Nature*.
500 2012;491(7422):119-24.
- 501 3. Zhang Y, Tian L, Sleiman P, Ghosh S, Hakonarson H, On behalf of the International IBDGC.
502 Bayesian analysis of genome-wide inflammatory bowel disease data sets reveals new risk loci.
503 *European Journal of Human Genetics*. 2018;26(2):265-74.
- 504 4. Sazonovs A, Stevens CR, Venkataraman GR, Yuan K, Avila B, Abreu MT, et al. Large-scale
505 sequencing identifies multiple genes and rare variants associated with Crohn's disease susceptibility.
506 *Nature Genetics*. 2022;54(9):1275-83.
- 507 5. Alatab S, Sepanlou SG, Ikuta K, Vahedi H, Bisignano C, Safiri S, et al. The global, regional, and
508 national burden of inflammatory bowel disease in 195 countries and territories, 1990-2017: a systematic
509 analysis for the Global Burden of Disease Study 2017. *The Lancet Gastroenterology & Hepatology*.
510 2020;5(1):17-30.
- 511 6. Morgan XC, Tickle TL, Sokol H, Gevers D, Devaney KL, Ward DV, et al. Dysfunction of the
512 intestinal microbiome in inflammatory bowel disease and treatment. *Genome Biology*. 2012;13(9):R79.
- 513 7. Gevers D, Kugathasan S, Denson LA, Vázquez-Baeza Y, Van Treuren W, Ren B, et al. The
514 treatment-naive microbiome in new-onset Crohn's disease. *Cell host & microbe*. 2014;15(3):382-92.
- 515 8. Lloyd-Price J, Arze C, Ananthakrishnan AN, Schirmer M, Avila-Pacheco J, Poon TW, et al.
516 Multi-omics of the gut microbial ecosystem in inflammatory bowel diseases. *Nature*.
517 2019;569(7758):655-62.

- 518 9. Ma S, Shungin D, Mallick H, Schirmer M, Nguyen LH, Kolde R, et al. Population structure
519 discovery in meta-analyzed microbial communities and inflammatory bowel disease using MMUPHin.
520 *Genome Biology*. 2022;23(1):208.
- 521 10. Duvallet C, Gibbons SM, Gurry T, Irizarry RA, Alm EJ. Meta-analysis of gut microbiome studies
522 identifies disease-specific and shared responses. *Nature Communications*. 2017;8(1):1784.
- 523 11. Sadlack B, Merz H, Schorle H, Schimpl A, Feller AC, Horak I. Ulcerative colitis-like disease in
524 mice with a disrupted interleukin-2 gene. *Cell*. 1993;75(2):253-61.
- 525 12. Dianda L, Hanby Am Fau - Wright NA, Wright Na Fau - Sebesteny A, Sebesteny A Fau -
526 Hayday AC, Hayday Ac Fau - Owen MJ, Owen MJ. T cell receptor-alpha beta-deficient mice fail to
527 develop colitis in the absence of a microbial environment. 1997(0002-9440 (Print)).
- 528 13. Sellon RK, Tonkonogy S, Schultz M, Dieleman LA, Grenther W, Balish E, et al. Resident enteric
529 bacteria are necessary for development of spontaneous colitis and immune system activation in
530 interleukin-10-deficient mice. *Infect Immun*. 1998;66(11):5224-31.
- 531 14. Aranda R, C. SB, McAllister PL, S.W. B, Yang HY, S.R. T, et al. Analysis of intestinal
532 lymphocytes in mouse colitis mediated by transfer of CD4+, CD45RBhigh T cells to SCID recipients.
533 1997(0022-1767 (Print)).
- 534 15. Vijay-Kumar M, Sanders CJ, Taylor RT, Kumar A, Aitken JD, Sitaraman SV, et al. Deletion of
535 TLR5 results in spontaneous colitis in mice. *J Clin Invest*. 2007;117(12):3909-21.
- 536 16. Schaubeck M, Clavel T, Calasan J, Lagkouvardos I, Haange SB, Jehmlich N, et al. Dysbiotic
537 gut microbiota causes transmissible Crohn's disease-like ileitis independent of failure in
538 antimicrobial defence. *Gut*. 2016;65(2):225.
- 539 17. Mazmanian SK, Round JL, Kasper DL. A microbial symbiosis factor prevents intestinal
540 inflammatory disease. *Nature*. 2008;453(7195):620-5.
- 541 18. Kim SC, Tonkonogy SL, Albright CA, Tsang J, Balish EJ, Braun J, et al. Variable phenotypes of
542 enterocolitis in interleukin 10-deficient mice monoassociated with two different commensal bacteria.
543 *Gastroenterology*. 2005;128(4):891-906.
- 544 19. Garrett WS, Gallini CA, Yatsunencko T, Michaud M, DuBois A, Delaney ML, et al.
545 Enterobacteriaceae Act in Concert with the Gut Microbiota to Induce Spontaneous and Maternally
546 Transmitted Colitis. *Cell Host & Microbe*. 2010;8(3):292-300.
- 547 20. Sokol H, Pigneur B, Watterlot L, Lakhdari O, Bermúdez-Humarán LG, Gratadoux J-J, et al.
548 *Faecalibacterium prausnitzii* is an anti-inflammatory commensal bacterium identified by gut microbiota
549 analysis of Crohn disease patients. *Proceedings of the National Academy of Sciences*.
550 2008;105(43):16731-6.
- 551 21. Gomes-Neto JC, Kittana H, Mantz S, Segura Munoz RR, Schmaltz RJ, Bindels LB, et al. A gut
552 pathobiont synergizes with the microbiota to instigate inflammatory disease marked by
553 immunoreactivity against other symbionts but not itself. *Scientific Reports*. 2017;7(1):17707.
- 554 22. Gilliland A, Chan J, De Wolfe TJ, Yang H, Vallance BA. Pathobionts in IBD: Origins, Underlying
555 Mechanisms, and Implications for Clinical Care. *Gastroenterology*. 2023.
- 556 23. Turnbaugh PJ, Ridaura VK, Faith JJ, Rey FE, Knight R, Gordon JI. The Effect of Diet on the
557 Human Gut Microbiome: A Metagenomic Analysis in Humanized Gnotobiotic Mice. *Science*
558 *Translational Medicine*. 2009;1(6):6ra14-6ra.
- 559 24. Ridaura VK, Faith JJ, Rey FE, Cheng J, Duncan AE, Kau AL, et al. Gut Microbiota from Twins
560 Discordant for Obesity Modulate Metabolism in Mice. *Science*. 2013;341(6150):1241214.
- 561 25. Routy B, Le Chatelier E, Derosa L, Duong CPM, Alou MT, Daillère R, et al. Gut microbiome
562 influences efficacy of PD-1-based immunotherapy against epithelial tumors. *Science*.
563 2018;359(6371):91-7.
- 564 26. Britton GJ, Contijoch EJ, Mogno I, Vennaro OH, Llewellyn SR, Ng R, et al. Microbiotas from
565 Humans with Inflammatory Bowel Disease Alter the Balance of Gut Th17 and RORγt+ Regulatory T
566 Cells and Exacerbate Colitis in Mice. *Immunity*. 2019;50(1):212-24.e4.

- 567 27. Sampson TR, Debelius JW, Thron T, Janssen S, Shastri GG, Ilhan ZE, et al. Gut Microbiota
568 Regulate Motor Deficits and Neuroinflammation in a Model of Parkinson's Disease. *Cell*.
569 2016;167(6):1469-80.e12.
- 570 28. Eun CS, Mishima Y, Wohlgemuth S, Liu B, Bower M, Carroll IM, et al. Induction of bacterial
571 antigen-specific colitis by a simplified human microbiota consortium in gnotobiotic interleukin-10^{-/-} mice.
572 *Infect Immun*. 2014;82(6):2239-46.
- 573 29. Rogala AR, Oka A, Sartor RB. Strategies to Dissect Host-Microbial Immune Interactions That
574 Determine Mucosal Homeostasis vs. Intestinal Inflammation in Gnotobiotic Mice. *Front Immunol*.
575 2020;11:214-.
- 576 30. Lengfelder I, Sava IG, Hansen JJ, Kleigrewe K, Herzog J, Neuhaus K, et al. Complex Bacterial
577 Consortia Reprogram the Colitogenic Activity of *Enterococcus faecalis* in a Gnotobiotic Mouse Model of
578 Chronic, Immune-Mediated Colitis. *Front Immunol*. 2019;10:1420-.
- 579 31. Cheng AG, Ho P-Y, Aranda-Díaz A, Jain S, Yu FB, Meng X, et al. Design, construction, and
580 in vivo augmentation of a complex gut microbiome. *Cell*. 2022;185(19):3617-36.e19.
- 581 32. Desai MS, Seekatz AM, Koropatkin NM, Kamada N, Hickey CA, Wolter M, et al. A Dietary Fiber-
582 Deprived Gut Microbiota Degrades the Colonic Mucus Barrier and Enhances Pathogen Susceptibility.
583 *Cell*. 2016;167(5):1339-53.e21.
- 584 33. Darfeuille-Michaud A, Neut C, Barnich N, Lederman E, Di Martino P, Desreumaux P, et al.
585 Presence of adherent *Escherichia coli* strains in ileal mucosa of patients with Crohn's disease.
586 *Gastroenterology*. 1998;115(6):1405-13.
- 587 34. Boudeau J, Glasser A-L, Masseret E, Joly B, Darfeuille-Michaud A. Invasive Ability of an
588 *Escherichia coli* Strain Isolated from the Ileal Mucosa of a Patient with Crohn's Disease. *Infect Immun*.
589 1999;67(9):4499-509.
- 590 35. Carvalho FA, Barnich N, Sivignon A, Darcha C, Chan CHF, Stanners CP, et al. Crohn's disease
591 adherent-invasive *Escherichia coli* colonize and induce strong gut inflammation in transgenic mice
592 expressing human CEACAM. *Journal of Experimental Medicine*. 2009;206(10):2179-89.
- 593 36. Federici S, Kredo-Russo S, Valdés-Mas R, Kviatcovsky D, Weinstock E, Matiuhin Y, et al.
594 Targeted suppression of human IBD-associated gut microbiota commensals by phage consortia for
595 treatment of intestinal inflammation. *Cell*. 2022;185(16):2879-98.e24.
- 596 37. Schmitz JM, Tonkonogy SL, Dogan B, Leblond A, Whitehead KJ, Kim SC, et al. Murine
597 Adherent and Invasive *E. coli* Induces Chronic Inflammation and Immune Responses in the Small and
598 Large Intestines of Monoassociated IL-10^{-/-} Mice Independent of Long Polar Fimbriae Adhesin A.
599 *Inflammatory Bowel Diseases*. 2019;25(5):875-85.
- 600 38. D'Adamo GL, Chonwerawong M, Gearing LJ, Marcelino VR, Gould JA, Rutten EL, et al.
601 Bacterial clade-specific analysis identifies distinct epithelial responses in inflammatory bowel disease.
602 *Cell Reports Medicine*. 2023;4(7).
- 603 39. Nagao-Kitamoto H, Shreiner AB, Gilliland MG, Kitamoto S, Ishii C, Hirayama A, et al.
604 Functional Characterization of Inflammatory Bowel Disease-Associated Gut Dysbiosis in Gnotobiotic
605 Mice. *Cellular and Molecular Gastroenterology and Hepatology*. 2016;2(4):468-81.
- 606 40. Heller F, Florian P, Bojarski C, Richter J, Christ M, Hillenbrand B, et al. Interleukin-13 Is the Key
607 Effector Th2 Cytokine in Ulcerative Colitis That Affects Epithelial Tight Junctions, Apoptosis, and Cell
608 Restitution. *Gastroenterology*. 2005;129(2):550-64.
- 609 41. Fuss IJ, Heller F, Boirivant M, Leon F, Yoshida M, Fichtner-Feigl S, et al. Nonclassical CD1d-
610 restricted NK T cells that produce IL-13 characterize an atypical Th2 response in ulcerative colitis. *J*
611 *Clin Invest*. 2004;113(10):1490-7.
- 612 42. Brand S. Crohn's disease: Th1, Th17 or both? The change of a paradigm: new immunological
613 and genetic insights implicate Th17 cells in the pathogenesis of Crohn's disease. *Gut*. 2009;58(8):1152.
- 614 43. Fouladi F, Glenn EM, Bulik-Sullivan EC, Tsilimigras MCB, Sioda M, Thomas SA, et al.
615 Sequence variant analysis reveals poor correlations in microbial taxonomic abundance between
616 humans and mice after gnotobiotic transfer. *ISME J*. 2020;14(7):1809-20.

- 617 44. Lundberg R, Toft MF, Metzdorff SB, Hansen CHF, Licht TR, Bahl MI, et al. Human microbiota-
618 transplanted C57BL/6 mice and offspring display reduced establishment of key bacteria and reduced
619 immune stimulation compared to mouse microbiota-transplantation. *Scientific Reports*.
620 2020;10(1):7805.
- 621 45. Chung H, Pamp Sünje J, Hill Jonathan A, Surana Neeraj K, Edelman Sanna M, Troy Erin B, et
622 al. Gut Immune Maturation Depends on Colonization with a Host-Specific Microbiota. *Cell*.
623 2012;149(7):1578-93.
- 624 46. Rawls JF, Mahowald MA, Ley RE, Gordon JI. Reciprocal Gut Microbiota Transplants from
625 Zebrafish and Mice to Germ-free Recipients Reveal Host Habitat Selection. *Cell*. 2006;127(2):423-33.
- 626 47. Goodman AL, Kallstrom G, Faith JJ, Reyes A, Moore A, Dantas G, et al. Extensive personal
627 human gut microbiota culture collections characterized and manipulated in gnotobiotic mice.
628 *Proceedings of the National Academy of Sciences*. 2011;108(15):6252-7.
- 629 48. Maharshak N, Packey CD, Ellermann M, Manick S, Siddle JP, Huh EY, et al. Altered enteric
630 microbiota ecology in interleukin 10-deficient mice during development and progression of intestinal
631 inflammation. *Gut Microbes*. 2013;4(4):316-24.
- 632 49. McCafferty J, Mühlbauer M, Gharaibeh RZ, Arthur JC, Perez-Chanona E, Sha W, et al.
633 Stochastic changes over time and not founder effects drive cage effects in microbial community
634 assembly in a mouse model. *ISME J*. 2013;7(11):2116-25.
- 635 50. Faith JJ, Ahern PP, Ridaura VK, Cheng J, Gordon JI. Identifying Gut Microbe–Host Phenotype
636 Relationships Using Combinatorial Communities in Gnotobiotic Mice. *Science Translational Medicine*.
637 2014;6(220):220ra11-ra11.
- 638 51. van der Lelie D, Oka A, Taghavi S, Umeno J, Fan TJ, Merrell KE, et al. Rationally designed
639 bacterial consortia to treat chronic immune-mediated colitis and restore intestinal homeostasis. *Nat*
640 *Commun*. 2021;12(1):3105.
- 641 52. Chassaing B, Srinivasan G, Delgado MA, Young AN, Gewirtz AT, Vijay-Kumar M. Fecal
642 Lipocalin 2, a Sensitive and Broadly Dynamic Non-Invasive Biomarker for Intestinal Inflammation. *PLoS*
643 *One*. 2012;7(9):e44328.
- 644 53. Rath HC, Herfarth HH, Ikeda JS, Grenther WB, Hamm TE, Jr., Balish E, et al. Normal luminal
645 bacteria, especially *Bacteroides* species, mediate chronic colitis, gastritis, and arthritis in HLA-
646 B27/human beta2 microglobulin transgenic rats. *J Clin Invest*. 1996;98(4):945-53.
- 647 54. Caporaso JG, Kuczynski J, Stombaugh J, Bittinger K, Bushman FD, Costello EK, et al. QIIME
648 allows analysis of high-throughput community sequencing data. *Nat Methods*. 2010;7(5):335-6.
- 649 55. Callahan BJ, McMurdie PJ, Rosen MJ, Han AW, Johnson AJA, Holmes SP. DADA2: High-
650 resolution sample inference from Illumina amplicon data. *Nat Methods*. 2016;13(7):581-3.
- 651 56. Rousta E, Oka A, Liu B, Herzog J, Bhatt AP, Wang J, et al. The Emulsifier
652 Carboxymethylcellulose Induces More Aggressive Colitis in Humanized Mice with Inflammatory Bowel
653 Disease Microbiota Than Polysorbate-80. *Nutrients*. 2021;13(10):3565.
- 654 57. Huttenhower C, Gevers D, Knight R, Abubucker S, Badger JH, Chinwalla AT, et al. Structure,
655 function and diversity of the healthy human microbiome. *Nature*. 2012;486(7402):207-14.
- 656 58. Halfvarson J, Brislawn CJ, Lamendella R, Vázquez-Baeza Y, Walters WA, Bramer LM, et al.
657 Dynamics of the human gut microbiome in inflammatory bowel disease. *Nature Microbiology*.
658 2017;2(5):17004.
- 659 59. Joossens M, Huys G, Cnockaert M, De Preter V, Verbeke K, Rutgeerts P, et al. Dysbiosis of the
660 faecal microbiota in patients with Crohn's disease and their unaffected relatives. *Gut*. 2011;60(5):631.
- 661 60. Hall AB, Yassour M, Sauk J, Garner A, Jiang X, Arthur T, et al. A novel *Ruminococcus gnavus*
662 clade enriched in inflammatory bowel disease patients. *Genome Medicine*. 2017;9(1):103.
- 663 61. Walter J, Armet AM, Finlay BB, Shanahan F. Establishing or Exaggerating Causality for the Gut
664 Microbiome: Lessons from Human Microbiota-Associated Rodents. *Cell*. 2020;180(2):221-32.
- 665 62. Winter SE, Lopez CA, Bäumlner AJ. The dynamics of gut-associated microbial communities
666 during inflammation. *EMBO reports*. 2013;14(4):319-27.

- 667 63. Taylor SJ, Winter MG, Gillis CC, Silva LAd, Dobbins AL, Muramatsu MK, et al. Colonocyte-
668 derived lactate promotes *E. coli* fitness in the context of inflammation-associated gut microbiota
669 dysbiosis. *Microbiome*. 2022;10(1):200.
- 670 64. Rojas-Tapias DF, Brown EM, Temple ER, Onyekaba MA, Mohamed AMT, Duncan K, et al.
671 Inflammation-associated nitrate facilitates ectopic colonization of oral bacterium *Veillonella parvula* in
672 the intestine. *Nature Microbiology*. 2022;7(10):1673-85.
- 673 65. Fornelos N, Franzosa EA, Bishai J, Annand JW, Oka A, Lloyd-Price J, et al. Growth effects of
674 N-acyl ethanolamines on gut bacteria reflect altered bacterial abundances in inflammatory bowel
675 disease. *Nature Microbiology*. 2020;5(3):486-97.
- 676 66. Zhang S, Morgan X, Dogan B, Martin F-P, Strickler S, Oka A, et al. Mucosal metabolites fuel the
677 growth and virulence of *E. coli* linked to Crohn's disease. *JCI Insight*. 2022;7(10).
- 678 67. Fischbach MA. *Microbiome: Focus on Causation and Mechanism*. *Cell*. 2018;174(4):785-90.
- 679 68. Lubin J-B, Green J, Maddux S, Denu L, Duranova T, Lanza M, et al. Arresting microbiome
680 development limits immune system maturation and resistance to infection in mice. *Cell Host & Microbe*.
681 2023;31(4):554-70.e7.
- 682 69. Tomofuji Y, Sonehara K, Kishikawa T, Maeda Y, Ogawa K, Kawabata S, et al. Reconstruction of
683 the personal information from human genome reads in gut metagenome sequencing data. *Nature*
684 *Microbiology*. 2023;8(6):1079-94.
- 685 70. Nina FdG, Britta CvB, Gerben M. Commercial DNA tests and police investigations: a broad
686 bioethical perspective. *Journal of Medical Ethics*. 2021;47(12):788.
- 687

688 **Tables**

689 **Supplementary Table S1:** Differential abundance analysis between groups excluding genera present
690 in less than 10% of the samples.

691

692 **Figure Legends**

693

694 **Figure 1. Mouse-adapted human microbiota induces more consistent and reproducible colitis**
695 **than directly transplanted human microbiota.** A) Experimental design. Pooled feces from 3 humans
696 with active IBD (2 CD, 1UC) were transplanted to non-inflamed WT or colitis-susceptible *Il-10^{-/-}* (IL-
697 10KO, KO) GF recipient mice. Mouse-adapted microbiotas were serial transplanted to non-inflamed WT
698 or colitis-susceptible *Il-10^{-/-}* GF recipient mice. B) Total colon and ileum histology score for WT mice at
699 day 28 post-colonization. C) f-LCN2 level at day 28 post-colonization. D) TNF α mRNA levels in cecal
700 tissue at day 28 post-colonization. E) Segment, total colon and ileum, and max segment histology score
701 for *Il-10^{-/-}* mice at day 28 post-colonization. F) Segment, total colon and ileum, and max segment
702 histology score for IMM-g1 colonized *Il-10^{-/-}* mice at day 28 post-colonization from 4 independent

703 experiments. Data shown are representative of (C-D) or cumulative (B, E-F) from 2-4 independent
704 experiments. n=7-9 (B-D), n=15-26 (E), n=5-8 (F) mice per group. Data are expressed as mean±SD or
705 geometric mean ± geometric SD (C). Statistical significance calculated by unpaired t-test or Mann-
706 Whitney test (C) with *p<0.05, **p<0.01, ***p<0.001.

707

708 **Supplemental Figure S1 (related to Figure 1). Mouse-adapted human microbiota induces more**
709 **consistent and reproducible colitis than directly transplanted human microbiota. A)**

710 Demographics and cohort membership of human IBD donors. B-D) f-LCN2 time-course of (B) HM1
711 colonized WT and KO mice, (C) NIMM-g1 colonized WT mice, (D) IMM-g1 or IMM-g2 colonized KO
712 mice. E-F) Bar plot (E) and Box-and-whisker (F) plot of segment histology score for HM1 and HM2
713 colonized KO mice at day 28 post-colonization. G) Box-and-whisker plot of segment histology score for
714 KO mice at day 28 post-colonization. H) Box-and-whisker plot of segment histology score for IMM-g1
715 colonized KO mice at day 28 post-colonization from 4 independent experiments. Data shown are
716 representative of (B-D, H) or cumulative (E-G) from 2-4 independent experiments. n=7-9 (B-D), n=11-
717 15 (E-F), n=15-26 (G), n=5-8 (H) mice per group. Data are expressed as mean±SD (E) or geometric
718 mean ± geometric SD (B-D). In box-and-whisker plots, box represents lower, median, and upper
719 quartiles; whiskers are min to max. Statistical significance calculated by Mann-Whitney test (B-D) or
720 unpaired t-test (E-H) with *p<0.05, **p<0.01, ***p<0.001.

721

722 **Figure 2. Recipient host environment influences engraftment composition of human-**

723 **microbiome associated mice. A) 16S Seq taxonomic bar plots show top 8 most abundant genera in**
724 **FMT inputs and recipient mouse feces at day 28 post-colonization. For mouse recipient groups, bar**
725 **plots are average of 16S seq data from n=7-18 mice/group.**

726

727 **Supplemental Figure S2 (related to Figure 2). Recipient host environment influences**
728 **engraftment composition of human-microbiome associated mice.** A) 16S Seq taxonomic bar plots
729 show top 8 most abundant genera in human and mouse-adapted FMT inputs and individual recipient
730 mouse feces at day 28 post-colonization. B) 16S Seq taxonomic bar plots show top 30 most abundant
731 genera in human and mouse-adapted FMT inputs and recipient mouse feces at day 28 post-
732 colonization. For mouse recipient groups, bar plots are average of 16S Seq data from n=7-18
733 mice/group.

734

735 **Figure 3. Human microbiome restructuring with transplant to GF mice is host inflammatory**
736 **environment specific.** A) Principal coordinates analysis, PCoA, of 16S Seq data for human and
737 mouse-adapted FMT inputs and FMT recipient WT and KO mouse groups. B) PCoA of FMT recipient
738 WT and KO mouse groups. C) PCoA of FMT recipient KO mouse groups. D) PCoA of FMT recipient
739 WT mouse groups. E) Shannon index at ASV level for FMT recipient WT and KO mouse groups. F)
740 Pearson correlation coefficients (r) within group for FMT recipient WT and KO mouse groups quantify
741 variability of microbiota composition between mice in the same group (microbiota engraftment
742 consistency). Dots in PCoA plots represent individual mice for FMT recipient WT and *Il-10^{-/-}* (KO)
743 mouse groups. For FMT inputs, a single input slurry was used in each experiment and input dots
744 represent sequencing data from three 16S amplicon PCR technical replicates. Analysis conclusions did
745 not change when using average input vs individual technical replicates, so technical replicates are
746 displayed to demonstrate the high consistency of 16S amplicon PCR in our dataset.

747

748 **Supplemental Figure S3 (related to Figure 3). Human microbiome restructuring with transplant**
749 **to GF mice is host inflammatory environment specific.** A) PCoA of 16S Seq data for HM1, HM2,
750 and mouse-adapted FMT inputs and FMT recipient KO mouse groups. B) Shannon index at genus level
751 for FMT recipient WT and KO mouse groups. C) Shannon index at ASV and genus level for HM1 and
752 HM2 FMT inputs. D) Pearson correlation coefficient (r) within group for HM1->KO and HM2->KO

753 recipient mouse groups quantifies variability of microbiota composition between mice in the same group
754 (microbiota engraftment consistency).

755

756 **Figure 4. Mouse-adapted human IBD microbiota transfers with higher efficiency than human**
757 **fecal transplant.** A) ASV level \log_{10} -normalized relative abundance correlations for FMT input and WT
758 recipient mice where each dot represents a unique ASV plotted in the input microbiome (x-axis) vs
759 recipient mouse microbiome (y-axis). B) Transfer efficiency quantified by Pearson correlation coefficient
760 (r) between FMT input and WT recipient mouse groups at the ASV level. C) ASV level \log_{10} -normalized
761 relative abundance correlations for FMT input and KO recipient mice. D) Transfer efficiency quantified
762 by Pearson correlation coefficient (r) between FMT input and KO recipient mouse groups at the ASV
763 level. E-J) Representative histograms of non-transferring ASVs (red, representing $y=0$ ASVs in above
764 dot plots) and newly detected *in vivo* ASVs (blue, representing $x=0$ ASVs in above dot plots) binned by
765 \log_{10} -normalized relative abundance for (E) HM1->WT, (F) NIMM-g1->WT, (G) NIMM-g2->WT, (H)
766 HM1->KO, (I) IMM-g1->KO, and (J) IMM-g2->KO FMT recipient mouse groups.

767

768 **Supplemental Figure S4 (related to Figure 4). Mouse-adapted human IBD microbiota transfers**
769 **with higher efficiency than human fecal transplant.** A-B) ASV level \log_{10} -normalized relative
770 abundance correlations comparing (A) HM1 input to NIMM-g1 input and (B) NIMM-g1 input to NIMM-g2
771 input. C) Pearson correlation coefficient (r) between HM1 input, NIMM-g1 input, and NIMM-g2 inputs at
772 the ASV level. D-E) ASV level \log_{10} -normalized relative abundance correlations comparing (D) HM1
773 input to IMM-g1 input and (E) IMM-g1 input to IMM-g2 input. F) Pearson correlation coefficient (r)
774 between HM1 input, IMM-g1 input, and IMM-g2 inputs at the ASV level. G) Pearson correlation
775 coefficient (r) between WT recipient and KO recipient groups at the ASV level.

776

777 **Figure 5. Transfer efficiency varies between taxa.** A) Genus-level and B) phylum-level \log_{10} -
778 normalized relative abundance correlations comparing HM1 input to HM1->KO, C-D) Pearson

779 correlation coefficient (r) between input and inflamed (KO) recipient at the (C) genus- and (D) phylum-
780 level. E) Genus-level and F) phylum-level log₁₀-normalized relative abundance correlations comparing
781 HM1 input to HM1->WT, G-H) Pearson correlation coefficient (r) between input and non-inflamed (WT)
782 recipient at the (G) genus- and (H) phylum-level. I-K) Pearson correlation coefficient (r) between input
783 and non-inflamed (WT) recipients by phylum. L-N) Pearson correlation coefficient (r) between input and
784 inflamed (KO) recipients by phylum.

785

786 **Supplemental Figure S5 (related to Figure 5). Transfer efficiency varies between taxa. A-C)**

787 Analysis of published 16S Seq data from Lundberg *et al.*⁴⁴ (A) Experimental design. Feces from a
788 single healthy human donor were transplanted to GF adult WT mice (Parent, P) in a gnotobiotic
789 isolator. HMA WT mice were bred in-isolator to generate F1 pups. B) ASV level log₁₀-normalized
790 relative abundance correlations for FMT input and recipient mice. For F1 pups, the input was natural
791 colonization by vertical transmission in-isolator from Parent (P). C) Transfer efficiency quantified by
792 Pearson correlation coefficient (r) between FMT input and recipient mouse groups at the ASV level. D)
793 Experimental design. Pooled feces from 3 humans with active IBD (3 CD, HM2) were transplanted to
794 colitis-susceptible *Il-10*^{-/-} (KO) GF recipient mice in a gnotobiotic isolator. E) ASV level log₁₀-normalized
795 relative abundance correlations for HM2 input and HM2->KO recipient mice. F) Table comparing
796 percentage shared OTU between input and recipient group at the ASV, Genus, and Phylum level.

797

798 **Figure 6. Inflamed mouse-adapted microbiome more rapidly induces severe colitis than non-**
799 **inflamed mouse adapted microbiome.** A). Experimental design. Human IBD patient microbiota (HM1)
800 was adapted in the inflamed (IMM-g1) or non-inflamed (NIMM-g1) host, then transplanted to *Il-10*^{-/-}
801 (KO) GF recipient mice. B) Segment and total colon + ileum histology score for KO mice at day 14 post-
802 colonization. C) Segment, total colon + ileum, and max segment histology score for KO mice at day 28
803 post-colonization. D) TNF α mRNA levels in cecal tissue at day 28 post-colonization. E) PCoA of FMT
804 recipient WT and KO mouse groups, including NIMM-g1->KO group. F) 16S Seq taxonomic barplots

805 show top 8 most abundant genera in FMT inputs and recipient mouse feces at day 28 post-
806 colonization. For mouse recipient groups, barplots are average of 16S seq data from n=7-18
807 mice/group. G) Shannon diversity index at ASV level for IMM-g1->WT, NIMM-g1->KO and NIMM-g1-
808 >WT groups. Data shown are representative of (D) or cumulative (B-C, E-F) from 2-4 independent
809 experiments. n=15-16 (B-C), n=5-8 (D), n=7-16 (E-G) mice per group. Data are expressed as
810 mean±SD. Statistical significance calculated by unpaired t-test (B-D, G) with *p<0.05, **p<0.01,
811 ***p<0.001, ****p<0.0001.

812

813 **Supplemental Figure S6 (related to Figure 6). Inflamed mouse-adapted microbiome more rapidly**
814 **induces severe colitis than non-inflamed mouse adapted microbiome.** A-C) f-LCN2 level of IMM-
815 g1->KO and NIMM-g1->KO mice at (A) day 14, (B) time-course from day 0 to day 14, and (C) day 28
816 post-colonization. D) 16S Seq taxonomic bar plots show top 30 most abundant genera in human and
817 mouse-adapted FMT inputs and recipient mouse feces at day 28 post-colonization. E-G) log₁₀-
818 normalized relative abundance of (E) *Blautia*, (F) *Lachnospiraceae NK4A136* group, (G) *R gnavus*
819 group, (H) *Hungatella* in NIMM-g1->KO vs NIMM-g1->WT mice. For mouse recipient groups, barplots
820 are average of 16S Seq data from n=7-18 mice/group. Data shown are cumulative (A) or representative
821 (B-C) of 2 independent experiments. n=15-16 (A), n=8-9 (B), n=7-8 (C) mice per group. Data are
822 expressed as geometric mean ± geometric SD (A-C). Statistical significance calculated by Mann-
823 Whitney test (A-C) or unpaired t-test (E-H) with *p<0.05, **p<0.01, ***p<0.001.

824

825 **Supplemental Information:**

826

827 **Supplemental File 1:** RMarkdown notebook of R Code Analysis and Jupyter Notebook of Python Code
828 Analysis. Also publicly available at [https://github.com/anhmoss/Mouse-Adaptation-of-Human-](https://github.com/anhmoss/Mouse-Adaptation-of-Human-Inflammatory-Bowel-Disease-Microbiota-Enhances-Colonization-Efficiency)
829 [Inflammatory-Bowel-Disease-Microbiota-Enhances-Colonization-Efficiency.](https://github.com/anhmoss/Mouse-Adaptation-of-Human-Inflammatory-Bowel-Disease-Microbiota-Enhances-Colonization-Efficiency)

830

831 **Supplemental Experimental Procedures**

832 **Gene expression by qRT-PCR**

833 Tissues were immediately placed in RNAprotect cell reagent to stabilize RNA. Total RNA extraction
834 from tissues (AllPrep PowerViral DNA/RNA Kit, Qiagen) and cDNA generation (iScript cDNA Synthesis
835 Kit, Bio-Rad) were performed according to the manufacturer's protocols. Quantitative RT-PCR was
836 performed on cDNA in duplicate or triplicate with a QuantStudio3 machine (ThermoFisher) using iTaq™
837 Universal SYBR Green Supermix (Bio-Rad). Target gene expression was quantified relative to internal
838 control b-actin and expressed using the comparative Ct method ($2^{-\Delta\Delta C_t}$). qPCR primer sequences are:
839 Tnfa-F 5'-ACCCTCACACTCAGATCATCTTCTC-3', Tnfa-R 5'-TGAGATCCATGCCGTTGG-3'. Actb-F
840 5'-AGCCATGTACGTAGCCATCCAG-3'; Actb-R 5'-TGGCGTGAGGGAGAGCATAG-3'

841 **Intestine histopathology scoring**

842 Small bowel and colon tissue sections were fixed in 10% phosphate-buffered formalin. Fixed tissue was
843 paraffin-embedded, sectioned at 5µm thickness, and stained with hematoxylin and eosin by the UNC
844 Center for Gastrointestinal Biology and Disease Histology Core. Histologic tissue inflammation was
845 quantified by blinded scoring as previously described on a scale of 0-4 for 5 tissue segments (terminal
846 ileum, cecum, proximal colon, distal colon, rectum)¹. Total inflammatory score was the summation of
847 the 5 segments. Max segment score was the single highest score from the 5 segments.

848 **Fecal lipocalin-2 quantification:**

849 Fecal samples (10-30mg) were homogenized in PBS with 0.1% Tween 20 and incubated at 4°C
850 overnight, followed by centrifugation to pellet solid debris. Lipocalin-2 ELISA was performed on clear
851 fecal supernatant according to manufacturer's instructions (DY1857, R&D Systems)².

852 **Microbial and Statistical Analyses**

853 16S rRNA amplicon (variable regions 3-4) PCR and sequencing were performed by the UNC
854 Microbiome Core. Sequencing was performed on an Illumina MiSeq platform. Sequencing outputs were

855 converted to fastq format and demultiplexed using Illumina Bcl2Fastq 2.20.0. The resulting paired-end
856 reads were processed with the QIIME2 2022-2 wrapper for DADA2 including merging paired ends,
857 quality filtering, error correction, and chimera detection^{3, 4}. Amplicon sequencing variants from DADA2
858 were assigned taxonomy with respect to the Silva databases, their sequences were aligned using
859 maFFT in QIIME2, and a phylogenetic tree was built with FastTree in QIIME2⁵⁻⁷.

860

861 **Supplemental References:**

- 862 1. Rath HC, Herfarth HH, Ikeda JS, Grenther WB, Hamm TE, Jr., Balish E, et al. Normal luminal
863 bacteria, especially *Bacteroides* species, mediate chronic colitis, gastritis, and arthritis in HLA-
864 B27/human beta2 microglobulin transgenic rats. *J Clin Invest*. 1996;98(4):945-53.
- 865 2. Chassaing B, Srinivasan G, Delgado MA, Young AN, Gewirtz AT, Vijay-Kumar M. Fecal
866 Lipocalin 2, a Sensitive and Broadly Dynamic Non-Invasive Biomarker for Intestinal Inflammation. *PLoS*
867 *One*. 2012;7(9):e44328.
- 868 3. Caporaso JG, Kuczynski J, Stombaugh J, Bittinger K, Bushman FD, Costello EK, et al. QIIME
869 allows analysis of high-throughput community sequencing data. *Nat Methods*. 2010;7(5):335-6.
- 870 4. Callahan BJ, McMurdie PJ, Rosen MJ, Han AW, Johnson AJA, Holmes SP. DADA2: High-
871 resolution sample inference from Illumina amplicon data. *Nat Methods*. 2016;13(7):581-3.
- 872 5. Quast C, Pruesse E, Yilmaz P, Gerken J, Schweer T, Yarza P, et al. The SILVA ribosomal RNA
873 gene database project: improved data processing and web-based tools. *Nucleic Acids Research*.
874 2013;41(D1):D590-D6.
- 875 6. Katoh K, Standley DM. MAFFT Multiple Sequence Alignment Software Version 7:
876 Improvements in Performance and Usability. *Molecular Biology and Evolution*. 2013;30(4):772-80.
- 877 7. Price MN, Dehal PS, Arkin AP. FastTree 2 – Approximately Maximum-Likelihood Trees for
878 Large Alignments. *PLoS One*. 2010;5(3):e9490.

Figure 1

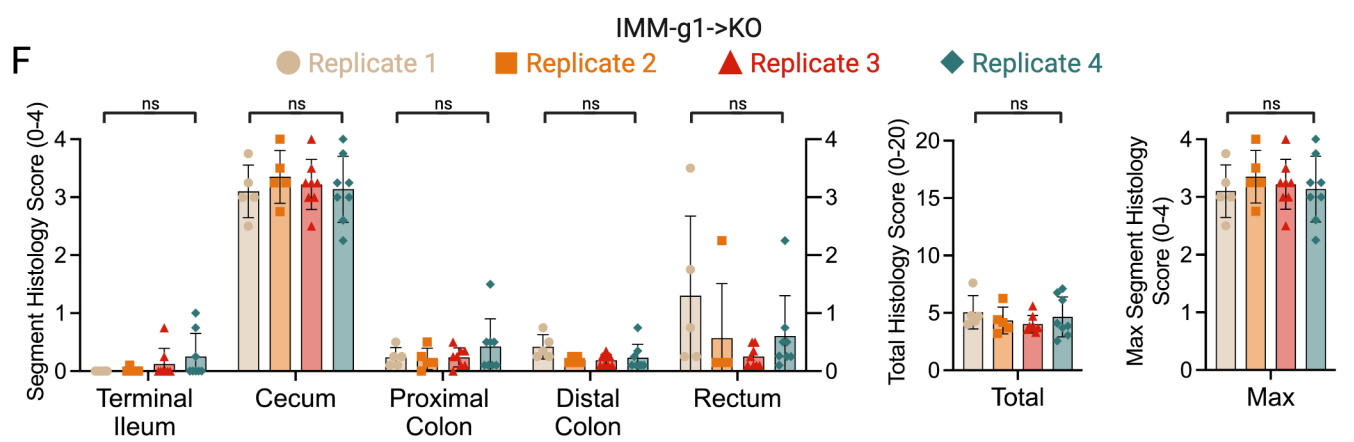
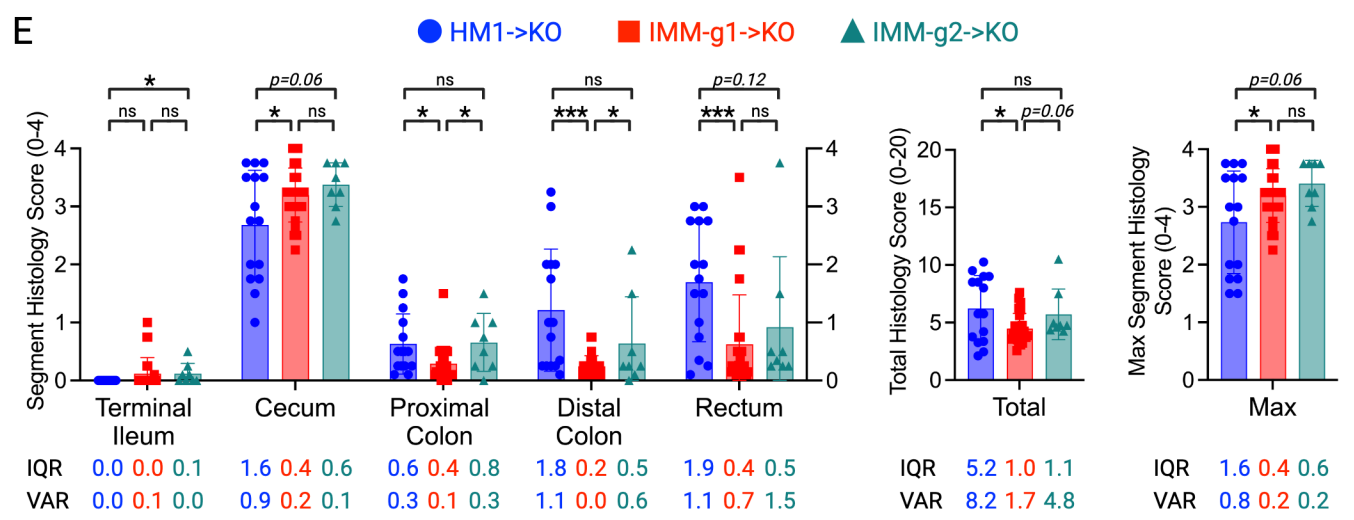
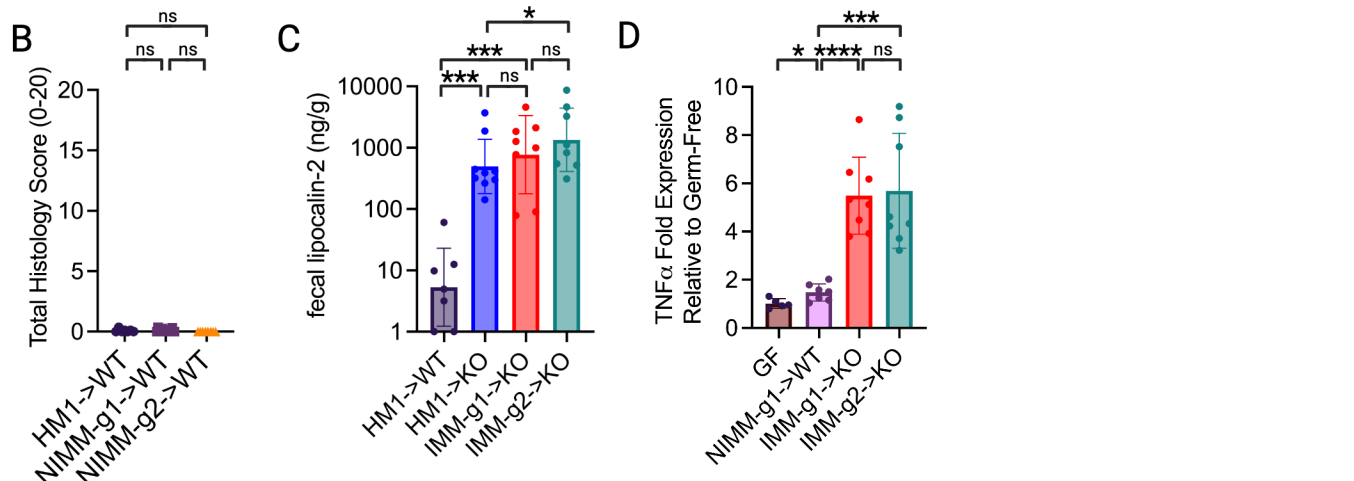
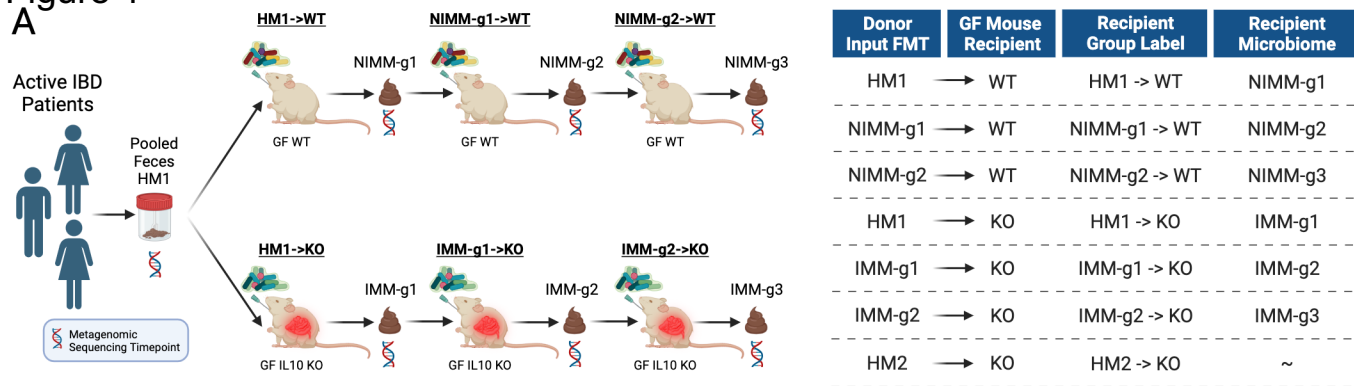
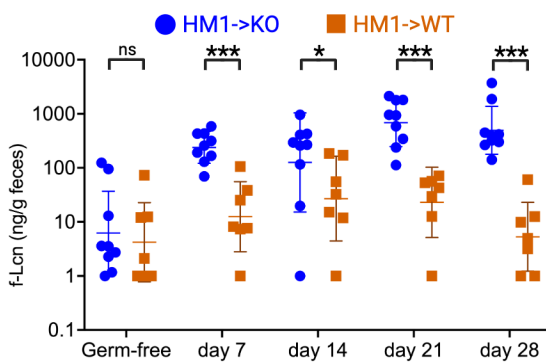


Figure S1, related to Figure 1

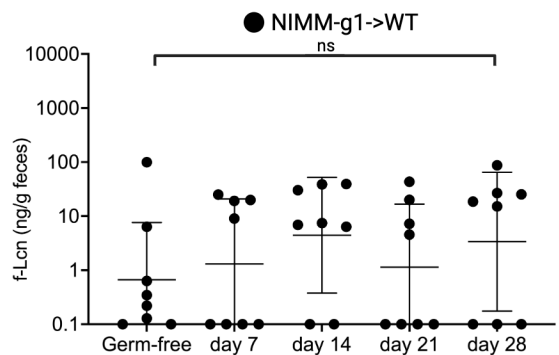
A

Human Donor ID	IBD Phenotype	Sex	Age (Decade)	Pooled Cohort
1	CD	M	50	HM1
2	UC	F	40	
3	CD	F	40	HM2
4	CD	M	40	
5	CD	F	60	

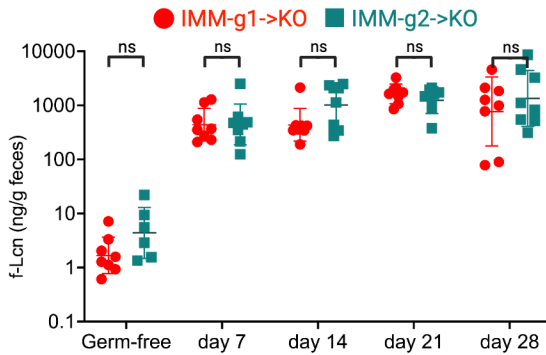
B



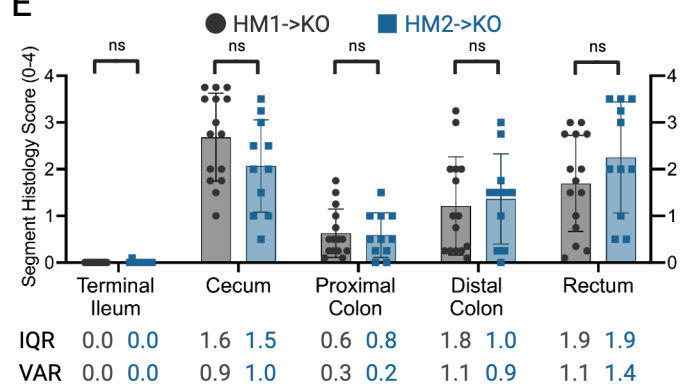
C



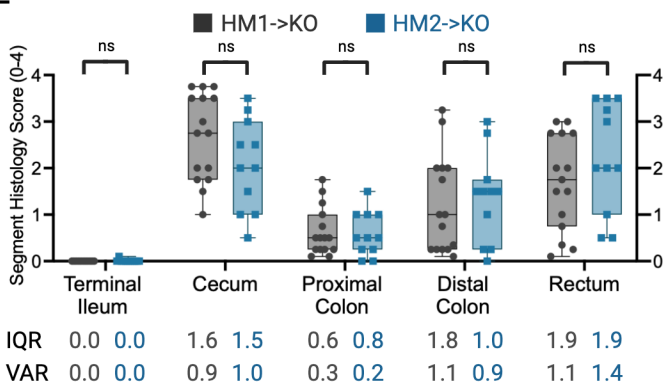
D



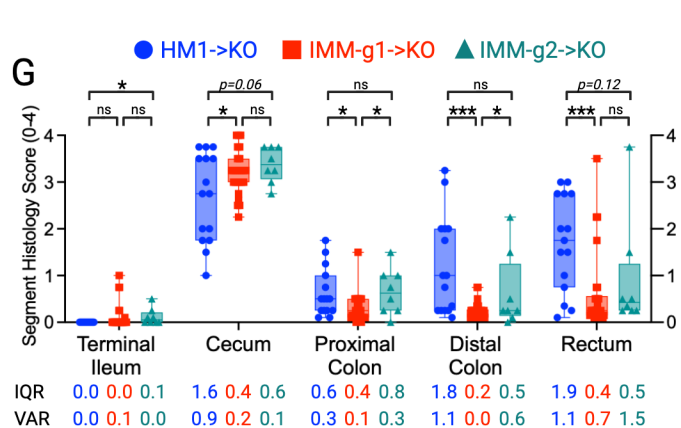
E



F



G



H

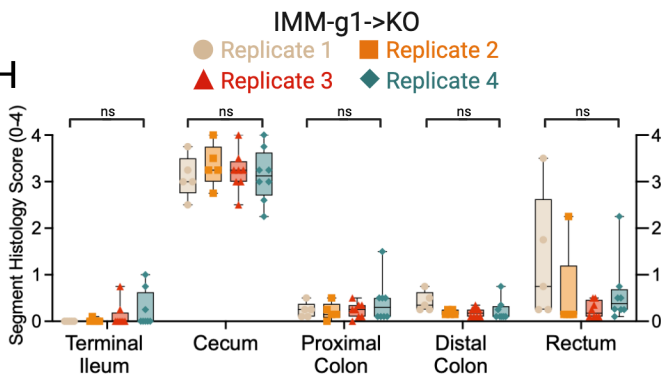
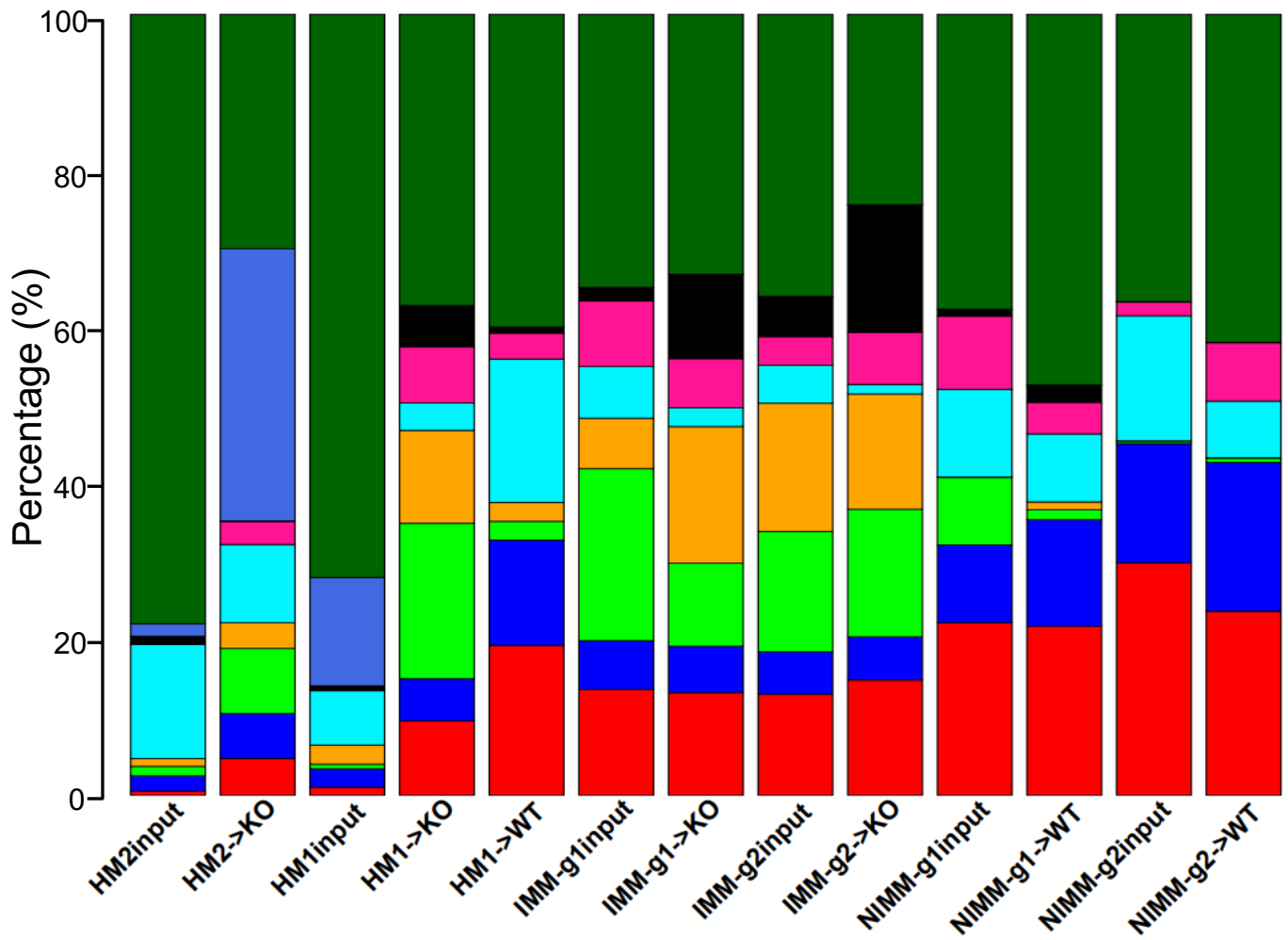


Figure 2



- Other
- d_Bacteria;p_Bacteroidota;c_Bacteroidia;o_Bacteroidales;f_Bacteroidaceae;g_Bacteroides
- d_Bacteria;p_Firmicutes;c_Clostridia;o_Clostridiales;f_Clostridiaceae;g_Clostridium_sensu_stricto_1
- d_Bacteria;p_Firmicutes;c_Clostridia;o_Lachnospirales;f_Lachnospiraceae;g_Hungatella
- d_Bacteria;p_Firmicutes;c_Clostridia;o_Lachnospirales;f_Lachnospiraceae;g_Blautia
- d_Bacteria;p_Proteobacteria;c_Gammaproteobacteria;o_Enterobacteriales;f_Enterobacteriaceae;g_Escherichia-Shigella
- d_Bacteria;p_Firmicutes;c_Clostridia;o_Lachnospirales;f_Lachnospiraceae;g_[Ruminococcus]_gnavus_group
- d_Bacteria;p_Firmicutes;c_Clostridia;o_Lachnospirales;f_Lachnospiraceae;g_Lachnoclostridium
- d_Bacteria;p_Verrucomicrobiota;c_Verrucomicrobiae;o_Verrucomicrobiales;f_Akkermansiaceae;g_Akkermansia

Figure S2, related to Figure 2

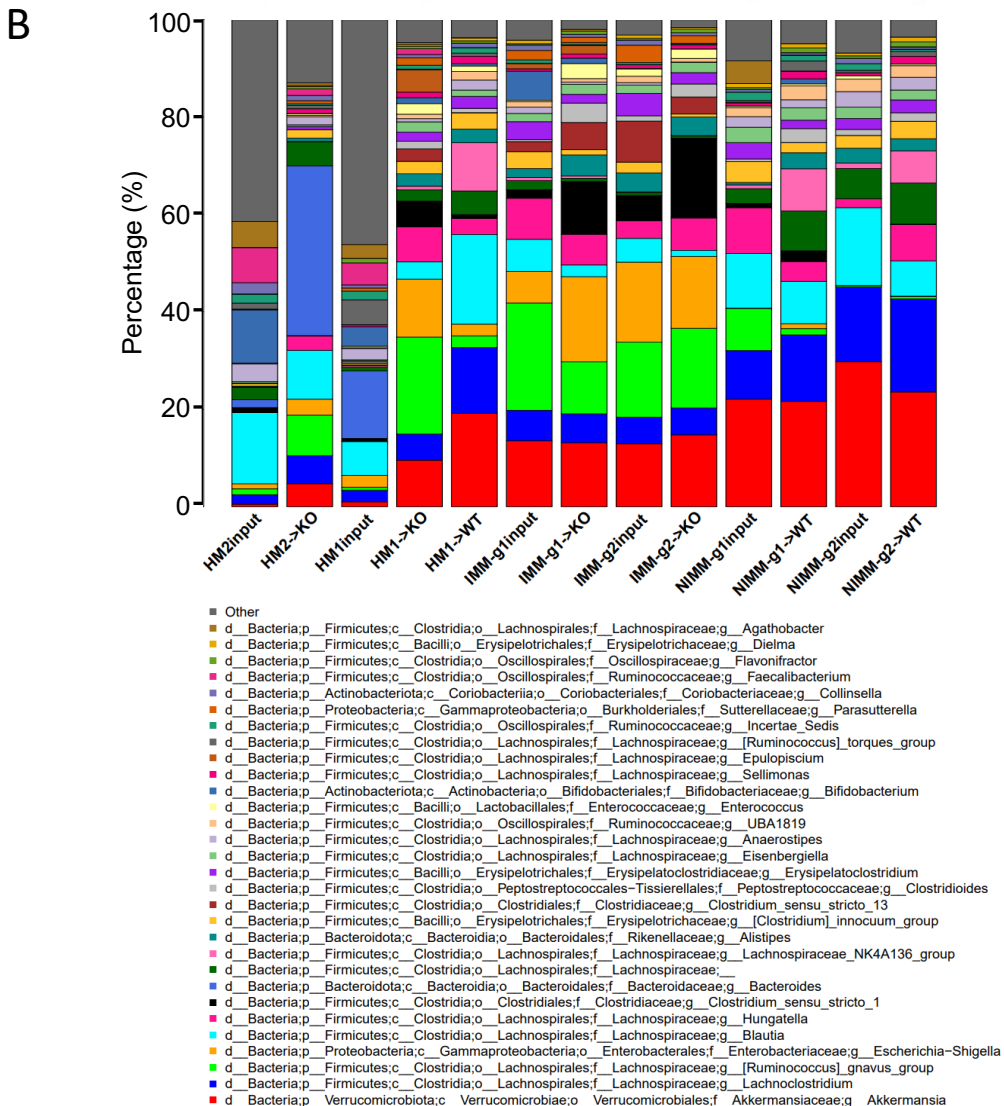
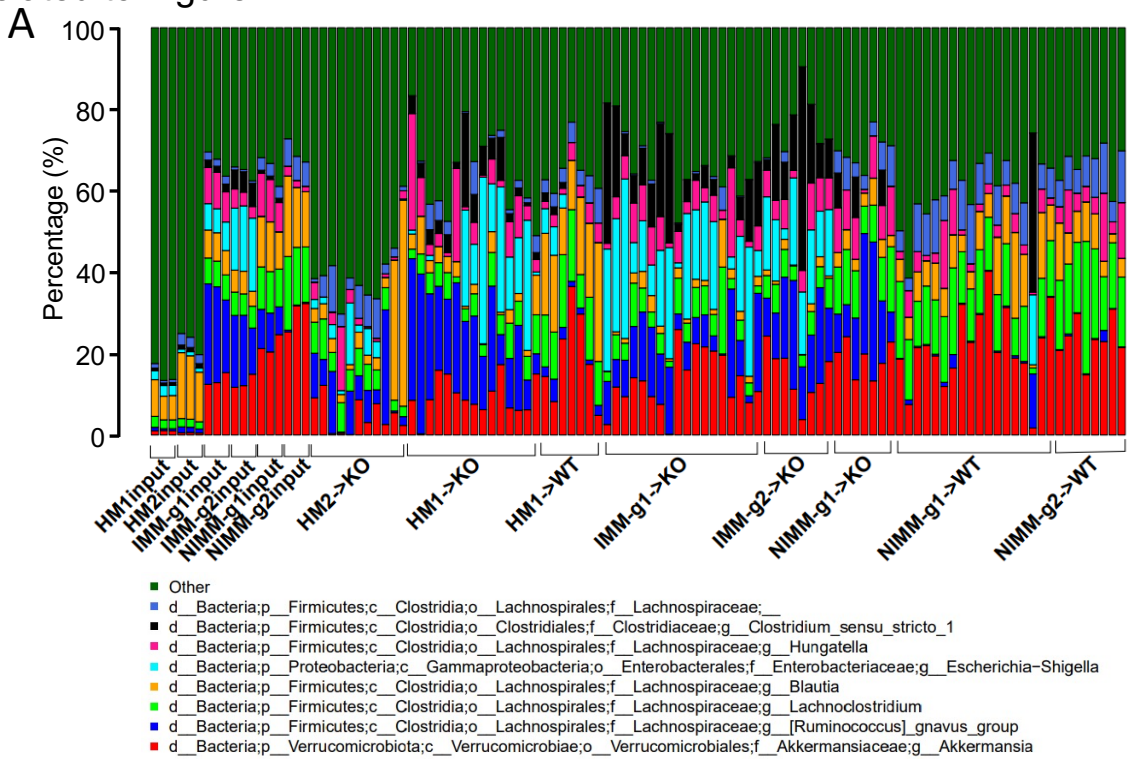
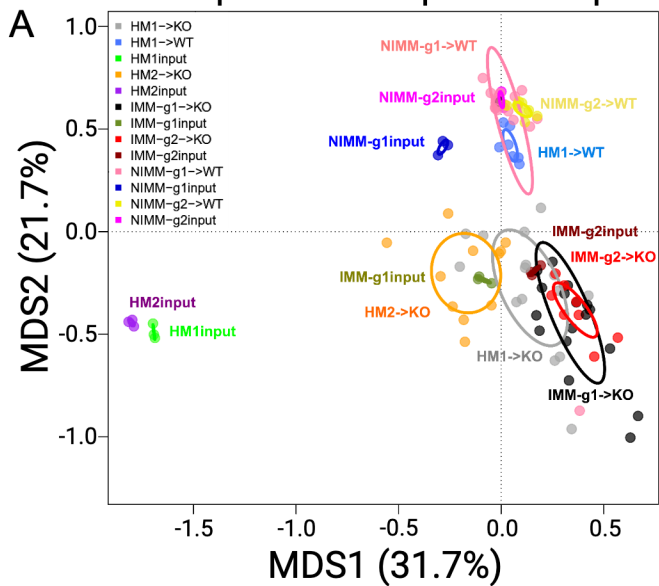
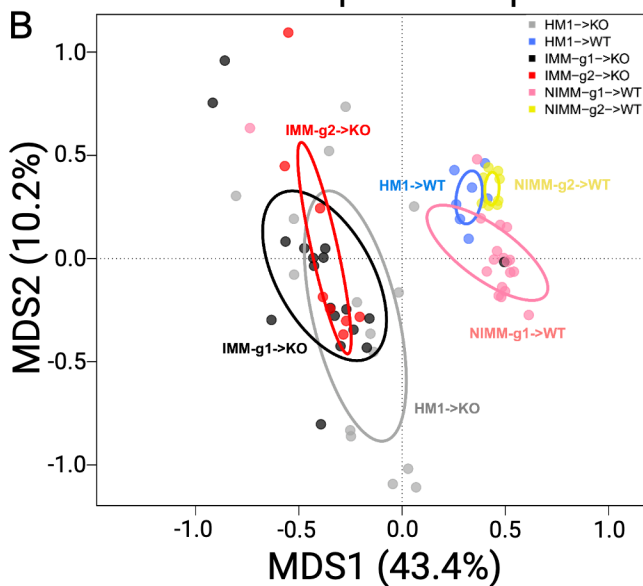


Figure 3

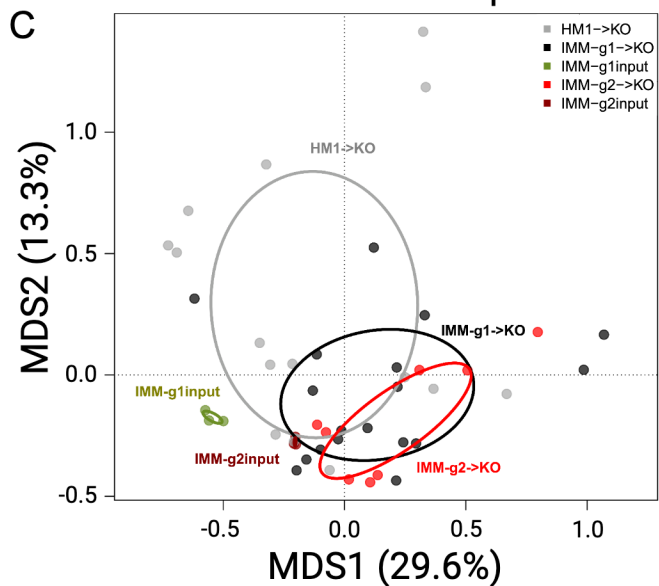
All Input and Recipient Groups



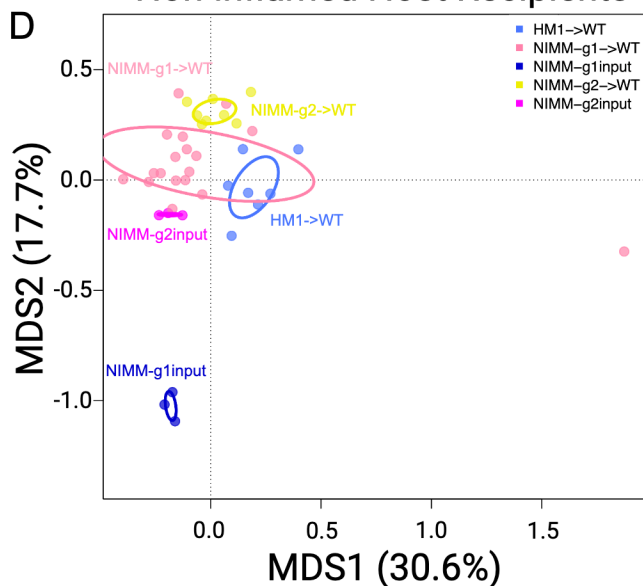
All Recipient Groups



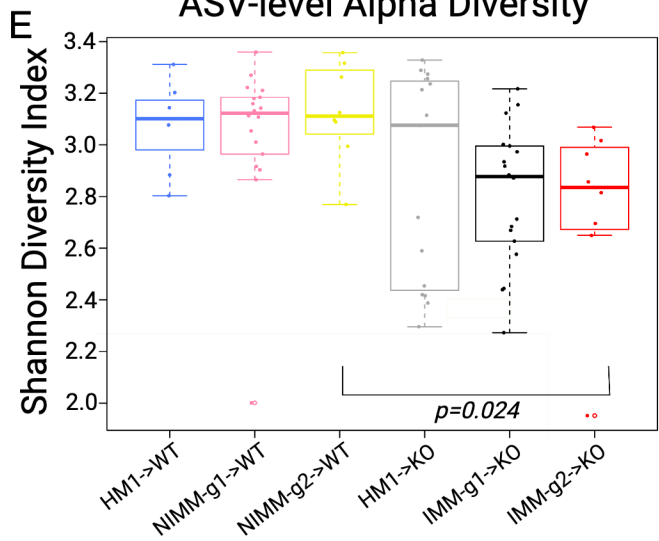
Inflamed Host Recipients



Non-inflamed Host Recipients



ASV-level Alpha Diversity



Microbiota Correlation within group

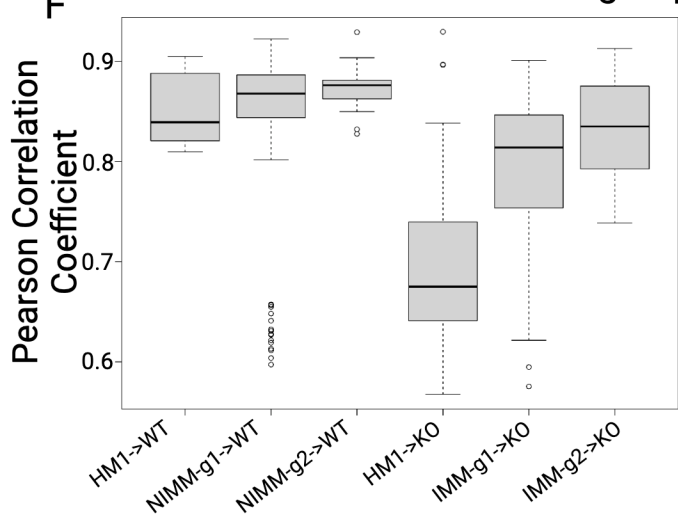
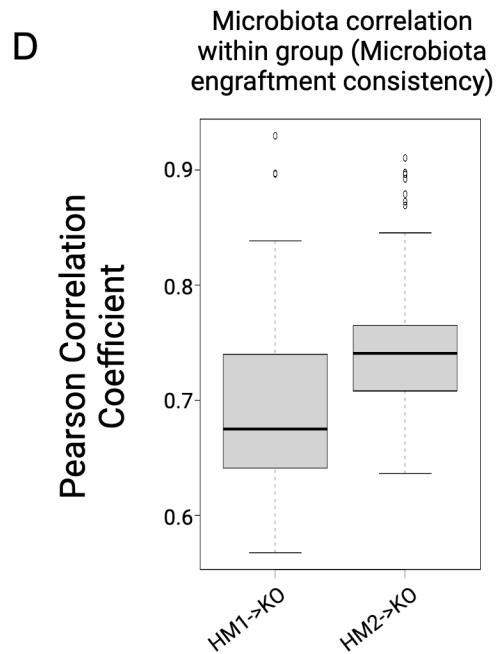
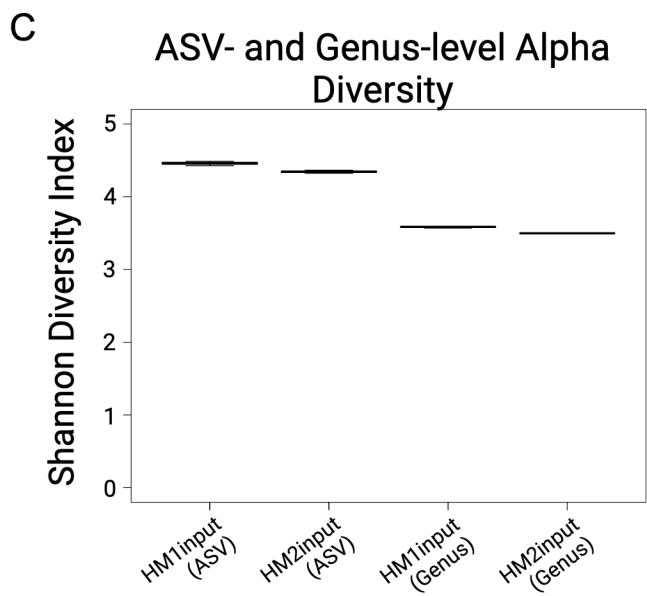
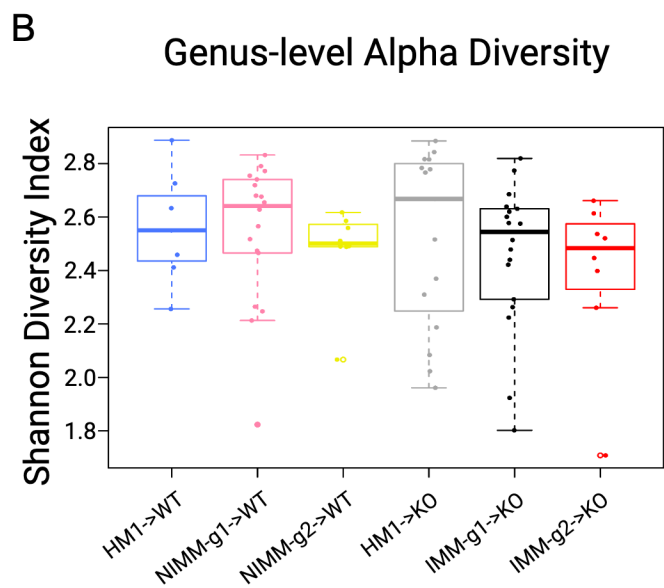
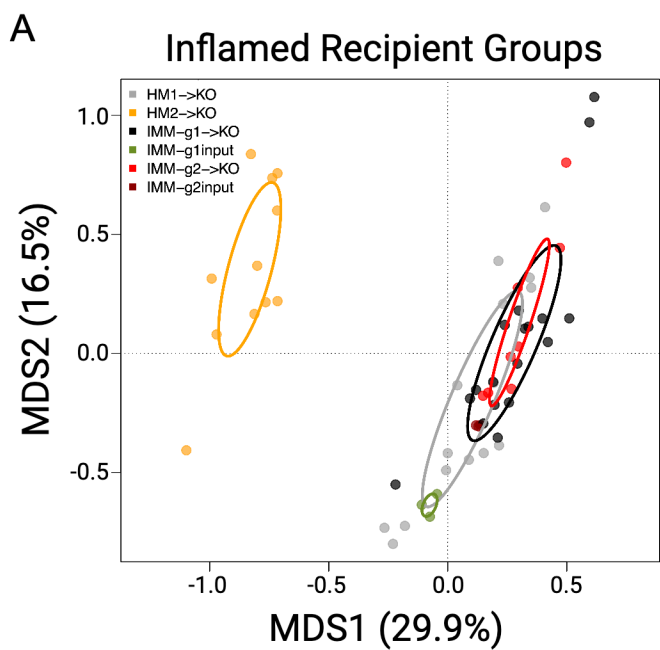


Figure S3, related to Figure 3



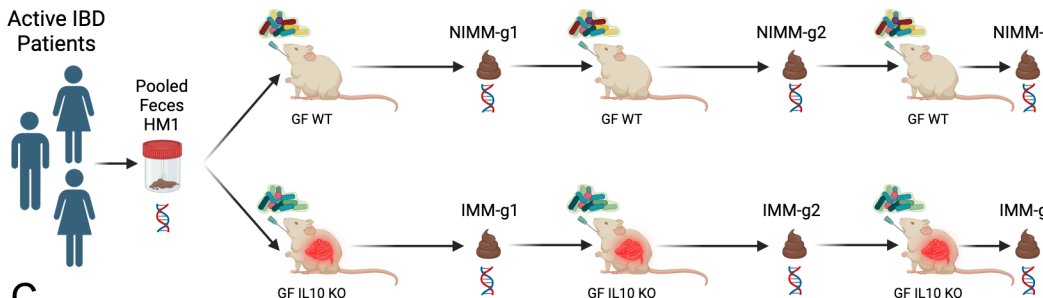
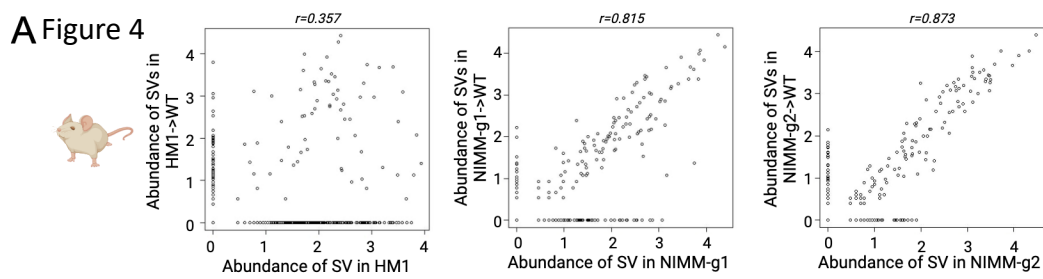
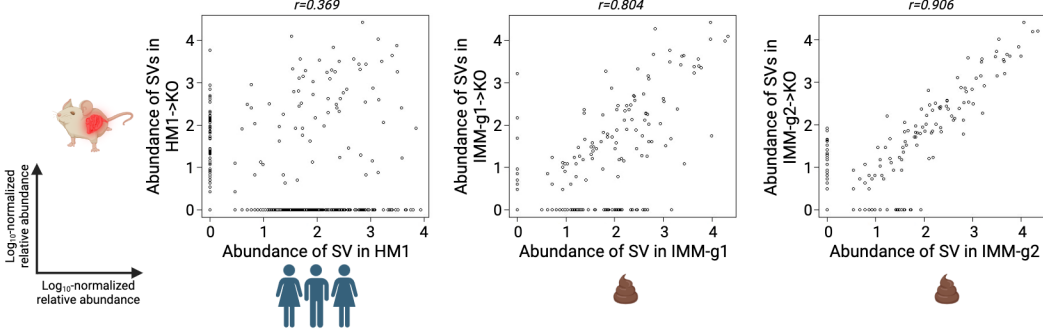
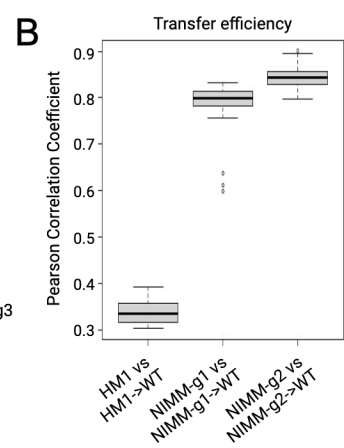
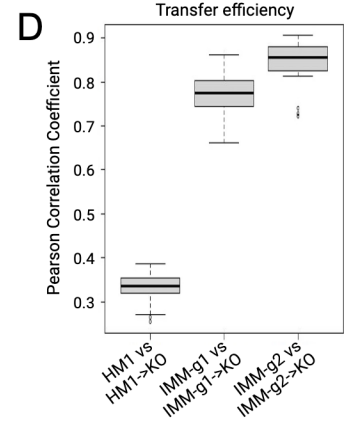
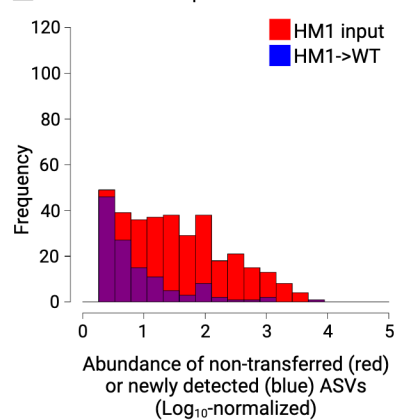
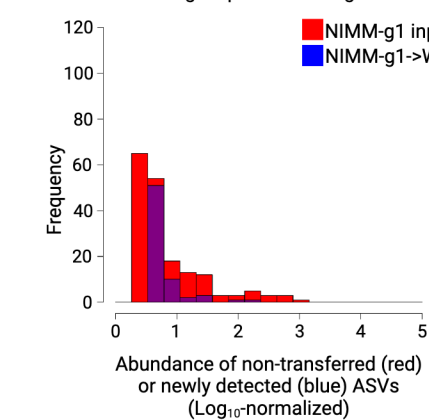
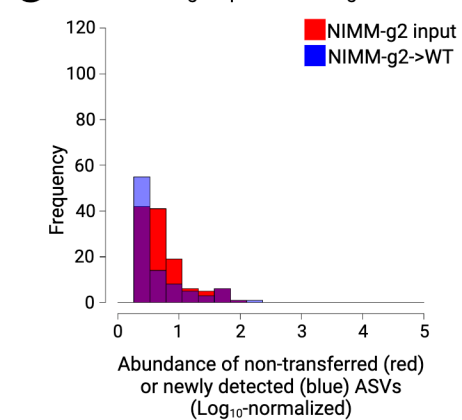
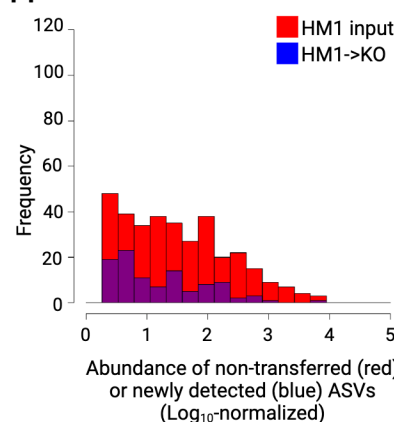
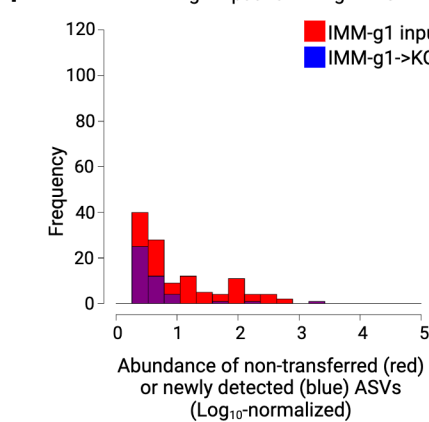
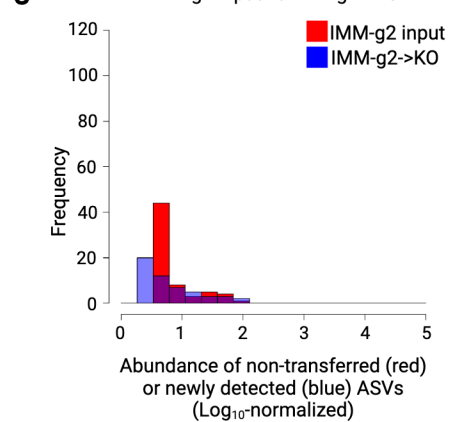
A Figure 4**C****B****D****E** HM1input vs HM1->WT**F** NIMM-g1 input vs NIMM-g1->WT**G** NIMM-g2 input vs NIMM-g2->WT**H** HM1input vs HM1->KO**I** IMM-g1 input vs IMM-g1->KO**J** IMM-g2 input vs IMM-g2->KO

Figure S4, related to Figure 4

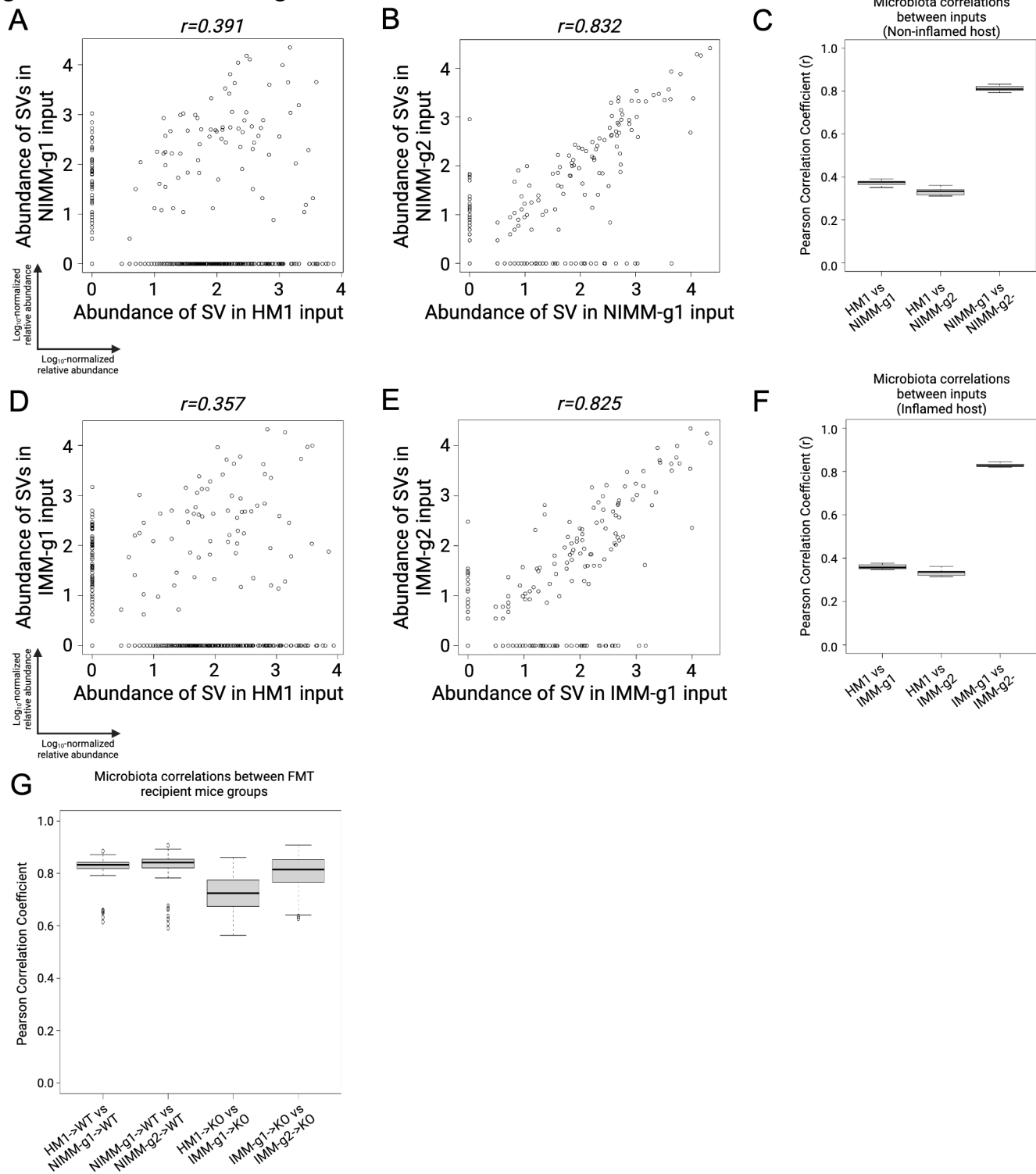


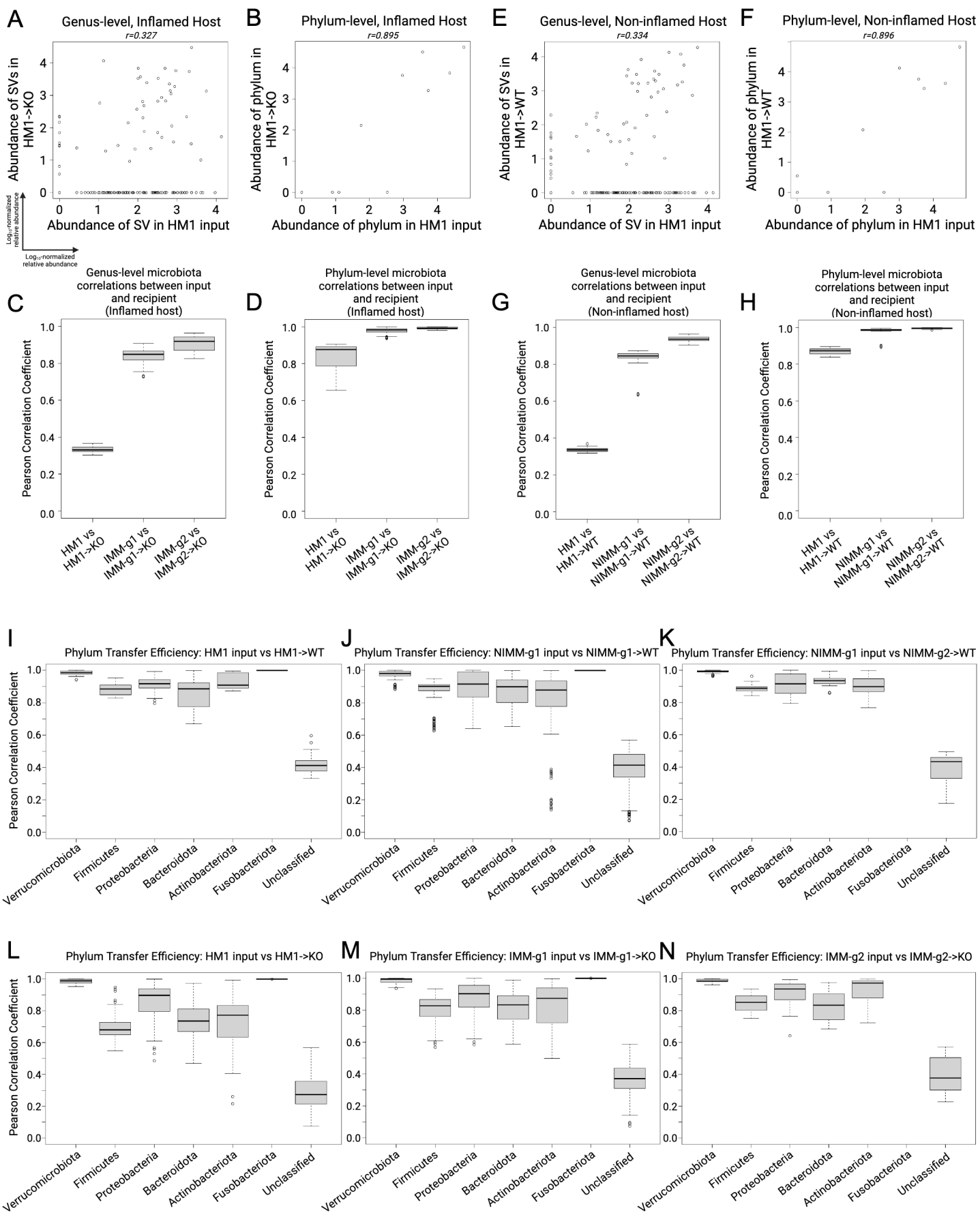
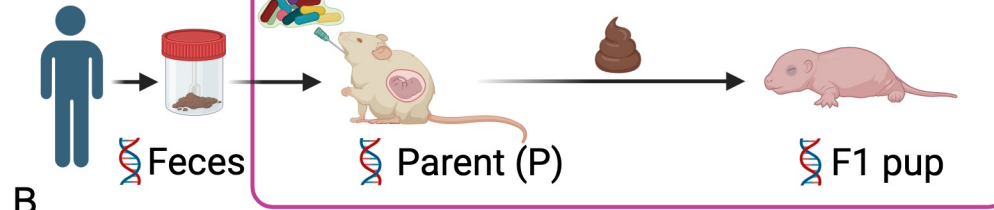
Figure 5

Figure S5, related to Figure 5

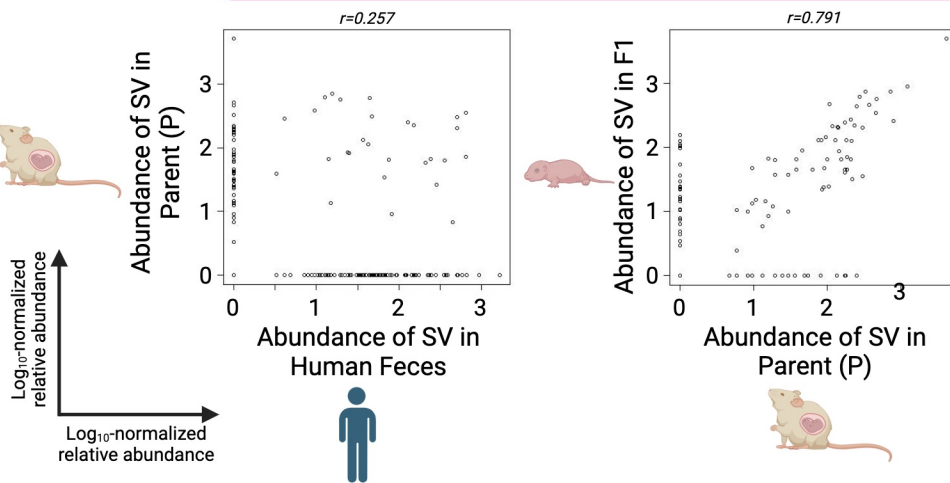
A

In Gnotobiotic Isolator

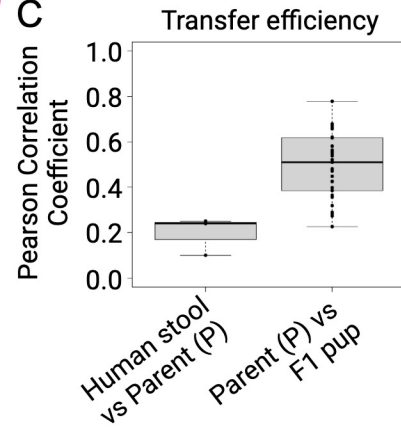
Healthy human



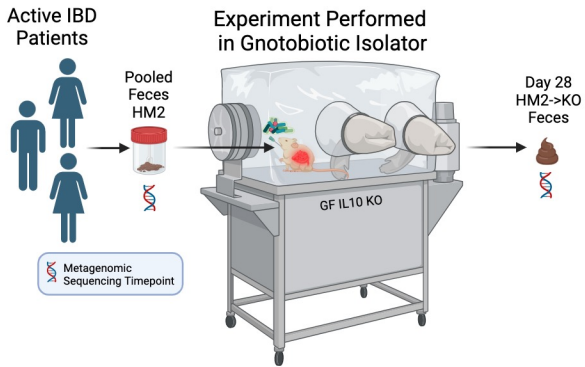
B



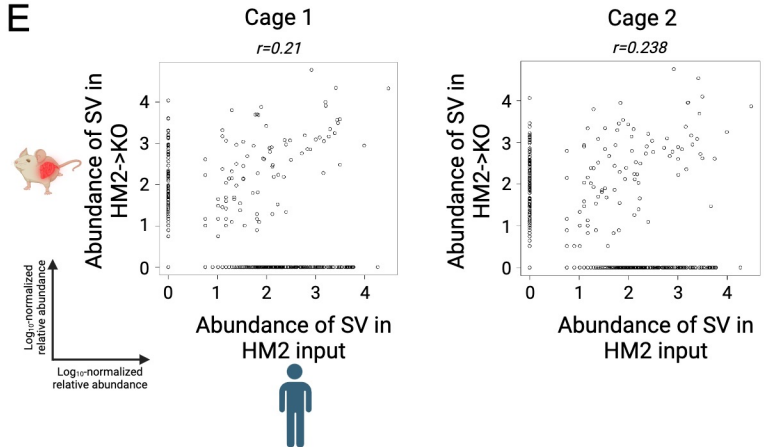
C



D



E



F

Percentage OTU Shared Between Donor Input and Recipient Group

Donor Input FMT	Recipient Group	% Shared ASV OTU	% Shared Genus OTU	% Shared Phylum OTU
HM1	HM1->WT	14.95%	31.36%	68.18%
HM1	HM1->KO	14.53%	30.73%	65.20%
HM2	HM2->KO	18.69%	32.25%	73.20%
IMM-g1	IMM-g1->KO	47.19%	69.63%	96.30%
IMM-g2	IMM-g2->KO	52.04%	80.91%	100%
NIMM-g1	NIMM-g1->WT	44.97%	71.93%	92.59%
NIMM-g2	NIMM-g2->WT	44.76%	84.74%	100%

Figure S6

